To the Graduate Council:

I am submitting herewith a thesis written by Edward Carmack Elder III entitled "A Comparative Experimental Study of Turbulence Reduction by Porous Honeycomb – A First Look." I have examined the final copy of this thesis for form and content and recommend that it be accepted in partial fulfillment of the requirements for the degree of Master of Science, with a major in Aerospace Engineering.

Dr. Ahmad D. Vakili, Major Professor

We have read this thesis
and recommend its acceptance:

Frank G. Collins

Roy J. Schulz

Accepted for the Council:

Interim Vice Provost and
Dean of The Graduate School

A Comparative Experimental Study of Turbulence Reduction by Porous Honeycomb – A First Look

A Thesis
Presented for the
Master of Science
Degree
The University of Tennessee

Edward Carmack Elder III
August 2001

Acknowledgements

I extend my thanks to the UTSI staff and especially my advisor, Dr. Vakili. As well as inventing the concept of this study, he provided outstanding support and encouragement that were instrumental in the success of this experiment and study. Dr. Collins and Dr. Schulz deserve credit for their support and advice in preparing my thesis. I also thank Mary Lo for her support in literature searches and Dr. Frank Steinle for his advice and making available to me a wealth of wind tunnel research papers. Tremendous obstacles were overcome in the manufacturing of the test articles and special thanks is therefore due to NASA Langley for their grant to conduct this experiment, to Gary Payne at the UTSI machine shop for his meticulous work in drilling holes in the honeycomb. The success of the test in the UTSI wind tunnel was due to the support of Jim Goodman and Keith Walker. Their tireless efforts were instrumental in insuring that all equipment functioned properly. Finally, I thank fellow student Abraham Meganathan for assisting in the particle image velocimetry.

Abstract

The purpose of this experiment and study was to analyze the effectiveness of porous-cell honeycomb at reducing large-scale turbulence generated from a cylinder placed upstream of the honeycomb and compare its performance to standard honeycomb. Particle image velocimetry (PIV) and hot-film anemometry measurement techniques were used to acquire data for the experiment. The objective of the particle image velocimetry test was to measure the velocity of (individual) smoke particles (seed) in the flow from which the vorticity and turbulence intensity contours of the flow could be obtained. The PIV also provided a means for flow visualization in this study. The objective of the hot-film anemometry test was to measure certain aspects of the velocity field, and from this data calculate velocity, turbulence intensity, and frequency spectrum information to determine the effectiveness of each honeycomb model at reducing flow non-uniformity and turbulence. The measured effectiveness of each honeycomb was used in a comparative analysis to determine the relative effectiveness of each porous honeycomb at turbulence reduction. The experiment collected performance data from a regular (solid wall) honeycomb, and a 20 percent, a 30 percent, and a 40 percent porous honeycomb. All tests were performed in the UTSI Low-Speed Wind Tunnel. The experiments were conducted at unit Reynolds number of nearly 350,000 (348,040) per foot. Both sets of measurements reveal that porous honeycomb may be superior to regular honeycomb at turbulence reduction.

Table of Contents

Chapter	Page
1. Introduction	1
2. Technical Background and Theoretical Considerations	3
3. Porous-Cell Honeycomb Design and Manufacturing	13
4. Particle Image Velocimetry Test	17
5. Velocity Field Measurements Using Hot Film Sensors	25
6. Conclusions and Recommendations	59
References	61
Appendices	63
A: Particle Image Velocimetry Calibration	64
B: Hot Film Calibration	65
Vita	70

List of Figures

Figure		Page
3-1	Regular (solid wall) Honeycomb	14
3-2	20% Porosity Honeycomb	14
3-3	30% Porosity Honeycomb	15
3-4	40% Porosity Honeycomb	15
4-1	PIV Camera and Laser Relative to Wind Tunnel	18
4-2	Diagram of PIV Test set Up	19
4-3	PIV Laser Flash	20
4-4	PIV Picture of Smoke Particles	21
4-5	PIV Turbulent Intensity Contours	23
4-6	PIV Instantaneous Vorticity Contours	24
5-1	Diagram of Hot Film Test	26
5-2	Test Section	27
5-3	Clean Tunnel Sensor 4 Velocity Statistics	31
5-4	Clean Tunnel Sensor 5 Velocity Statistics	31
5-5	Cylinder No Honeycomb Sensor 4 Velocity Statistics	32
5-6	Cylinder No Honeycomb Sensor 5 Velocity Statistics	32
5-7	Regular Honeycomb Sensor 4 Velocity Statistics	33
5-8	Regular Honeycomb Sensor 5 Velocity Statistics	33
5-9	20% Porosity Honeycomb Sensor 4 Velocity Statistics	34
5-10	20% Porosity Honeycomb Sensor 5 Velocity Statistics	34

5-11	30% Porosity Honeycomb Sensor 4 Velocity Statistics	35
5-12	30% Porosity Honeycomb Sensor 5 Velocity Statistics	35
5-13	40% Porosity Honeycomb Sensor 4 Velocity Statistics	36
5-14	40% Porosity Honeycomb Sensor 5 Velocity Statistics	36
5-15	Data Delta Between Sensors 4 and 5	37
5-16	Clean Tunnel Velocity Sensor 4 Run 4	39
5-17	Cylinder No Honeycomb Velocity Sensor 4 Run 5	39
5-18	Clean Tunnel Turbulence Intensity Sensor 4 Run 4	40
5-19	Cylinder No Honeycomb Turbulence Intensity Sensor 4 Run 5	40
5-20	Comparison of Cylinder No Honeycomb to Regular Honeycomb Velocity	42
5-21	Comparison of Cylinder No Honeycomb to Regular Honeycomb Turbulence Intensity	43
5-22	Comparison of Cylinder No Honeycomb to 20% Porosity Honeycomb Velocity	44
5-23	Comparison of Cylinder No Honeycomb to 20% Porosity Honeycomb Turbulence Intensity	46
5-24	Comparison of Cylinder No Honeycomb to 30% Porosity Honeycomb Velocity	47
5-25	Comparison of Cylinder No Honeycomb to 30% Porosity Honeycomb Turbulence Intensity	48

5-26	Comparison of Cylinder No Honeycomb to 40% Porosity Honeycomb Velocity	50
5-27	Comparison of Cylinder No Honeycomb to 40% Porosity Honeycomb Turbulence Intensity	51
5-28	Average Percent Turbulence Intensity for Sensor 4	52
5-29	Average Percent Turbulence Intensity for Sensor 5	52
5-30	Comparison of Frequency Spectrum Averages of Sensor 4, 0-100 Hz	54
5-31	Comparison of Frequency Spectrum Averages of Sensor 4, 0-25 Hz	54
5-32	Comparison of Frequency Spectrum Averages of Sensor 5, 0-100 Hz	56
5-33	Comparison of Frequency Spectrum Averages of Sensor 5, 0-25 Hz	56
5-34	NonPorous Length to Honeycomb Length	57
B-1	Hot Film Sensor and Velocity Components	66
B-2	Sensor 4 Calibration Curve and Raw Data	68
B-3	Sensor 5 Calibration Curve and Raw Data	68
B-4	Sensor 6 Calibration Curve and Raw Data	69

List of Symbols

TI	Turbulence intensity
$\overline{U}'$	Time mean average of velocity
$\overline{U}$	Time mean average of velocity in x direction
ΔP	Change in static pressure
K	pressure-loss coefficient
f_{tr}	turbulence reduction factor
q	dynamic pressure
ρ	Fluid density
Re	Reynolds number
K_o	$\left(1-0.95B/0.95B\right)^2$
Re_d	Reynolds number based on wire diameter
B	Projected open area/ Total area = $(1\text{-}d/M)^2$
d	wire diameter
M	mesh length
F1	Prandtl's equation for axial turbulence
F2	Dryden and Schubauer equation for lateral turbulence
L	Honeycomb cell length
D_{cd}	Cell diameter
δ	Boundary layer height
x	distance
V	Fluid velocity
Re_x	Reynolds number based on distance x

μ	Fluid viscosity
D_{EPA}	Length from leading edge to end of porous area
D_{LHC}	Length of honeycomb cell
D_{CCD}	Center-to-center spacing
U	Velocity behind honeycomb
U_∞	Free stream velocity
f	Frequency of flow oscillations behind honeycomb
f_∞	Free stream frequency of flow oscillations
A_p	Porous area
A_t	Total Area
A_s	Shape area
D_{wad}	Width relative to axial flow direction
D_{ldd}	Length relative to axial flow direction
F_1	Pi function of dimensional analysis with all terms
F_2	Pi function of dimensional analysis with nondimensional terms
F_3	Pi function of dimensional analysis with terms relative to experiment
ξ	Vorticity
∇	Del
V	Velocity vector
ν	Kinematic viscosity
St	Strouhal number
Hz	Hertz

U_i	Velocity in x direction (axial), where "i" is one data sample
U'_i	Fluctuating velocity in the x direction
N	Number of data samples
Σ	Summation
τ	Standard deviation
MTI	Mean turbulence intensity

Chapter 1

Introduction

Experimental information obtained from wind tunnel tests continues to play a significant role in aerodynamic test and evaluation methods despite increased capabilities in numerical modeling and simulation techniques. Tight schedules and lower budgets require that adequate quantities of high quality test data be obtained from wind tunnel test facilities in as few tests as possible. This requires test facilities to become more efficient by reducing operating cost and test time and increasing the quality of data provided to customers. Major operating costs consist of electric power, maintenance, and labor costs. It is well known that reducing the turbulence in a wind tunnel test section results in improved flow quality. Typical wind tunnel turbulence reduction systems (TRS) consist of combinations of wire-mesh screens and honeycomb. A new type of honeycomb, porous-cell honeycomb has been invented at UTSI [1. Dr. Ahmad D. Vakili] that has the potential to increase test section flow quality. If it increases test section flow quality, then it can potentially reduce the number of wire mesh screens which are prone to generating turbulence if not maintained. Also, maintenance cost for multi-layered screens is very labor intensive and increases operating costs.

This study is an experimental investigation on the effectiveness of porous honeycomb at increasing test section flow quality by increasing turbulence reduction. The thesis is that porous honeycomb will improve the velocity profile in the test section by allowing variations in the flow field to be smoothed out because of lateral communication of the

flow between adjacent cells in the honeycomb, and thus create a more evenly distributed velocity profile for the test section. In other words, total pressure and temperature distortions can laterally diffuse in the flow between honeycomb cells. This study begins with a literature review and technical considerations for TRS in Chapter 2. The design and manufacturing of the porous-cell honeycomb is explained in Chapter 3. Chapter 4 contains the experimental testing of regular (non-porous) and porous honeycomb, and analysis of the particle image velocimetry data. Chapter 5 contains the results and analysis of the hot film test. Finally, Chapter 6 contains conclusion and recommendations concerning the effectiveness of the new honeycomb and design.

Chapter 2

Technical Background and Theoretical Considerations

The test section of a wind tunnel is where data is collected on test articles and therefore, the nature of the flow in this section without the test article present must meet specific criteria and its performance must be known. Typical test section performance criteria are defined in terms of velocity vectors, and turbulence intensity, temperature and pressure levels in the empty test section. If the nature of the flow field is not known or checked periodically, disturbances may be present that will create what are called "interference errors" or bias errors on the test data and can thus lead to incorrect engineering designs with costly consequences, especially to commercial aircraft or military weapon systems.

The flow quality in an empty test section for an ideal case would be a uniform velocity profile with parallel streamlines headed downstream. This translates into no lateral velocity components and turbulence for an empty test section.

All known wind tunnels require a TRS in their inlets to reduce sources of non-ideal flow in the test section. Potential sources of non-ideal flow in wind tunnel inlets for closed-circuit tunnels are corner turning vanes, diffusers, contraction nozzles, contraction ratio, wall irregularities, fan and compressor blades, vibrations, and pressure leaks. TRS can itself create additional sources of turbulent flow if not functioning properly.

Literature Review of Turbulence Reduction Systems

The most common TRS consist of combinations of wire-mesh screen and honeycomb to create the required flow quality for the test section. Flow quality is typically quantified by the level of turbulence or turbulence intensity and is expressed as follows [2. Munson, p. 476]:

$$TI = (\sqrt{\overline{U'}} / \overline{U})$$

where,

$\sqrt{\overline{U'}}$ = square root of the mean square of the fluctuating velocity

and

$\overline{U}$ = time mean average.

This equation and concept is explained in greater detail in the hot-film analysis approach section of Chapter 5.

A well-designed tunnel can achieve turbulence intensity of 0.01 and with extreme care, intensity as low as 0.0002 can be obtained [2. Munson, p. 476]. The design flow quality parameters for the European Transonic Wind tunnel are: turbulence intensity of 0.0005 and flow angularity of +/- 0.1 degree [3. Bouis, p. 11-2]. The study on developing requirements for the National Wind tunnel Complex yielded flow quality requirements for flow angularity +/- 0.1 degree and turbulence intensity of less than 0.0005 [4. Brines, p. 29].

Wire-mesh screens function as TRS by transforming larger scale turbulence to that of the size of the screen openings plus vorticies generated from the flow past each wire. The smaller vorticies generated from flow over the screen wire dissipate to heat sooner

than the larger vortices. The mechanism for homogenizing the flow and reducing scale of turbulence is pressure loss (ΔP) across the screen. The pressure of a pressure loss across a screen means that the screen presents an obstacle to flow in the axial direction. Local regions of higher pressure force the flow to distribute itself laterally. For screens, the larger the blockage or the pressure loss, the greater the ability to reduce lateral disturbances. Screens used in TRS should have a ratio of projected open area to total area greater than 0.57 because with ratios below 0.57, test section flow suffers from flow instabilities [5. Rae, p. 76].

A common approach to the theoretical analysis of screens is based on a pressure-loss coefficient (K) and a turbulence reduction factor (f_{tr}). For screens, K is defined as the pressure loss across the screen divided by the dynamic pressure (q) of the mean flow through the screen and is expressed as follows [5. Rae, p. 76]:

$K=\Delta P/q = \Delta P/ (0.5 \rho \overline{U}^2)$.

K can be expressed in terms screen geometry and Reynolds number (Re) as follows [5. Rae, p. 76]:

$K=K_o + 55.2/ Re_d$

where,

$$K_o = \left(1 - 0.95B \Big/ 0.95B\right)^2$$

and,

B = Projected open area/ Total area = $(1-d/M)^2$

d=wire diameter

M=mesh length

Re_d = Reynolds number based on wire diameter, d

The turbulence reduction factor can be expressed in axial components, and lateral components [5. Rae, p. 77]. For the axial direction, Prandtl's equation for turbulence reduction is expressed as:

$F1 = 1/(1+K)$

In the lateral direction, the Dryden and Schubauer equation is expressed as:

$F2 = \sqrt{F1}$.

As a wind tunnel flow passes into a honeycomb section, it is discretized into a series of parallel, pressure-driven pipe flows. If there are pressure variations across the flow, its discretization by the honeycomb divides the flow into smaller individual flows, each having a slightly different inlet pressure. This isolation of the pipe flows into separate pipe flows allows the walls of each cell to act as a barrier to lateral flow disturbances. The walls also allow a boundary layer to grow from the surface of each honeycomb cell wall. If the honeycomb length is long enough, its boundary layer will become fully developed. Because the flow entering the honeycomb is turbulent, the boundary layer will quickly become turbulent. The cell walls and boundary layer growth have the effect of reducing the large-scale lateral turbulence to a maximum scale the size of the honeycomb cell diameter. This smaller scale turbulence and the turbulence generated from flow exiting the honeycomb will dissipate much sooner than the larger scale turbulence present without the honeycomb. The lateral turbulent velocities are, therefore, reduced due the effect of discretization and boundary layer growth in each honeycomb cell.

A study by J. L. Lumley [6. Lumley, p. 218-220] on the effect of honeycomb or cell length-to-diameter (L/D_{cd}) ratio on turbulence reduction concluded that in order to reduce lateral velocity components, the flow in the honeycomb cells must be fully developed turbulent flow. This fully developed flow would in most cases be turbulent due to the turbulent flow entering the cells and due to imperfections in honeycomb manufacturing acting as a trip for turbulent flow. Lumley's study assumed that if transition occurred at a length Reynolds number of 10^5 and if the diameter Reynolds number was greater than 2000, then the boundary layer would grow according to the following turbulent flat plate boundry layer equation:

$$\delta / x = 0.37 \mathrm{Re}_x^{-1/5}$$

For fully developed flow, $\delta = D_{cd}/2$

Where,

δ = boundary layer height

D_{cd} = cell diameter

x = distance

V=fluid velocity

$$\mathrm{Re}_x = \rho V x / \mu$$

The relation,

$$\delta / x = 0.37 \mathrm{Re}_x^{-1/5}$$

can be rearranged in terms of the length and diameter required for fully developed flow and can be expressed as follows:

$$x^{4/5} / D \geq (1.35)\left(\rho V / \mu\right)^{1/5}$$

Lumley's study did not provide a definition of what range of L/ D_{cd} constitutes a large L/ D_{cd}. However, based on Figure 2. in his paper, and the fact that he tested a honeycomb with a L/ D_{cd} of 32, the large L/ D_{cd} range appears to begin at 20-to-30. To achieve the same turbulence reduction with significantly less pressure loss, Lumley concluded that one honeycomb is equivalent to four screens with a blockage of 0.45.

Another honeycomb study by R. I. Loehrke and H. M. Nagib [7. Loehrke and Nagib, p. 342-353] noted that in literature searches, a considerable amount of theoretical and experimental information is available on the effect of screens on turbulence. However, the literature available on the effect of honeycomb on turbulent flow fields is limited in spite of their extensive use in wind and water tunnels. Loehrke and Nagib's test used honeycomb models constructed with different lengths of straws of the same diameter. Their results indicate that as cell length increases, the boundary layer is more developed and, therefore, the jet that exits each honeycomb cell is wider. This increased wake or mixing area between jets creates larger shear layer instabilities between adjacent cells. Loehrke and Nagib also placed a screen behind their straw models and their results indicate increased turbulence reduction. Their results conclude that for reduction of free-stream turbulence in wind or water tunnels, optimum performance is achieved with combinations of honeycomb and screens and in particular a screen downstream of the honeycomb. The distance downstream should not exceed a distance of L/ D_{cd} = 5. They also recommend that the optimum honeycomb L/ D_{cd} is 11.

Additional literature reviews concluded that honeycomb is without a doubt an effective method of turbulence reduction. However, Lumley recommended large L/D_{cd} and Loehrke and Nagib recommended relatively short L/D_{cd}, there does not appear to be a set of universally adopted empirical or theoretical equations to predict and compare honeycomb and honeycomb plus screen performance.

Theory of Porous-Cell Honeycomb

Dr. Ahmad D. Vakili [1. Dr. Ahmad D. Vakili] developed a concept for improved honeycomb performance by considering a porous-walled honeycomb design. The theory of how porous-walled honeycomb functions was based on each cell wall having holes that create flow passages between cells. It was envisioned [1. Dr. Ahmad D. Vakili] that the holes in each cell wall allow the total pressure differential to equilibrate, or balance between adjacent cells. This would have the effect of averaging the total pressure differential between adjacent cells. By averaging the total pressure between adjacent cells, both axial and lateral disturbances are reduced in the porous-walled honeycomb section. However, since flow exchange between cells could create additional disturbances to the flow it was also postulated that the porous section should be located as near the honeycomb cell entrance as possible. This would allow the nonporous part of each cell to perform the traditional role of eliminating lateral turbulence just before exiting the honeycomb.

An additional advantage of the improved performance of porous honeycomb to reduce flow disturbances would be that its use should reduce the number of screens required to

achieve a desired level of test section flow quality. It is desirable to eliminate as many inlet screens as possible because they tend to vibrate and flex over the large cross-sectioned flow areas in stilling chambers. This flexing creates additional sources of flow angularity and turbulence. Screens also tear, which increases maintenance cost. Fewer screens would reduce pressure losses and therefore, increase operating efficiency.

Dimensional Analysis

Dimensional analysis helps the experimentalist deduce which dimensionless groups of process variables correlate with the behavior or functionality of the system, thus complex systems with many variables can be surveyed or controlled by much smaller, more manageable number of process variables. Also, through the concept of similitude, a system of both dynamic and geometric similarity, results from a lab prototype can be applied through empirical formulations to systems of larger or smaller scale. In order to take advantage of the similitude concept, system variables are transformed into dimensionless groups or products of the controlling variables. The dimensionless products allow empirical formulations to be developed from experiments and applied to system simulations.

The relevant system or process variables for the incompressible experiments of this study are as follows:

ρ = Density

μ = Viscosity

D_{cd} = Cell diameter

D_{EPA}= Length from leading edge to end of porous area

D_{LHC}= length of honeycomb cell

D_{CCD} = Center-to-center spacing

U= Velocity behind honeycomb

U_∞ = Free stream velocity

f = Frequency of flow oscillations behind honeycomb

f_∞ = Free stream frequency of flow oscillations

A_p = Porous area

A_t= Total Area

A_s = Shape area

D_{wad} = Width relative to axial flow direction

D_{ldd} = Length relative to axial flow direction

The relationship between the geometric characteristics of the honeycomb and the velocity downstream of the honeycomb can be expressed as a function (F_1) as follows:

$$F_1(\rho, \mu, D_{cd}, D_{EPA}, D_{LHC}, D_{CCD}, U, U_\infty, f, f_\infty, A_p, A_t, A_s, D_{wad}, D_{ldd}) = 0$$

By employing the Buckingham Pi Theorem [2. Munson, p398], this system of 15 variables can be reduced to 12, using the primary dimensions of mass, length and time along with the repeating variables (μ, U, D_{LHC}), dimensionless variables and expressed in the following function (F_2):

$$F_2\left(\frac{\rho U D_{LHC}}{\mu}, \frac{D_{cd}}{D_{LHC}}, \frac{D_{EPA}}{D_{LHC}}, \frac{D_{CCD}}{D_{LHC}}, \frac{U_\infty}{U}, \frac{f D_{LHC}}{U}, \frac{f_\infty D_{LHC}}{U}, \frac{A_s}{D_{LHC}^2}, \frac{D_{wad}}{D_{LHC}}, \frac{D_{ldd}}{D_{LHC}}, \frac{A_p}{D_{LHC}^2}, \frac{A_t}{D_{LHC}^2}\right) = 0$$

For this experiment, the amount of porous area, A_p, between the cells of the honeycomb was varied from zero (nonporous) to a maximum of 40 percent of the total area of the cell walls. This, A_p determined the length from leading edge of the honeycomb to end of porous area, for each test. For each value of A_p, the resulting velocity behind honeycomb, U, and frequency of flow oscillations behind honeycomb, f, was measured. This experiment can be reduced to six Pi terms that change due the change in honeycomb porosity. The variables that change are U, D_{EPA}, f, and A_p. A function (F_3) in terms of Pi terms with variables that change as a result of changing porosity in this experiment is as follows:

$$F_3\left(\frac{\rho U D_{LHC}}{\mu}, \frac{D_{EPA}}{D_{LHC}}, \frac{U_\infty}{U}, \frac{fD_{LHC}}{U}, \frac{f_\infty D_{LHC}}{U}, \frac{A_p}{D_{LHC}^2}\right) = 0.$$

Thus a system with 12 Pi terms is reduced to one of 6 Pi terms.

Chapter 3

Porous Honeycomb Design and Manufacturing

Four honeycomb models were manufactured and analyzed. Three of the four honeycombs have porosity. The theory of how porous honeycomb operates dictated that holes in the walls be near one edge. The fabrication process began by acquiring metal sheets from Kentucky Metals located in New Albany, Indiana. The dimensions of the stainless steel sheets were 16- by 6- by 0.005 inches. Figures 3-1, 3-2, 3-3 and 3-4 show the design of each porous honeycomb tested.

The UTSI machine shop did an outstanding job of drilling holes in the sheets. Sheets were clamped every 3 inches with a 3/8-inch sheet of aluminum on top and bottom to firmly secure the thin stainless steel sheets before they were drilled. Great care was taken during the drilling of each hole. There was concern that if the drill were forced down too hard or quickly, shear stresses would tear the sheets or create burrs. Several machine shops determined that drilling holes in the 0.005 inch thick sheets to create the specified hole pattern would not work due to shear stresses tearing the sheets. The drilled sheets were then sent back to Kentucky Metals for fabrication into honeycomb. The sheets were stacked to maximize hole line up between sheets and a spot weld held each sheet in place. Table 3-1 has specific dimensions and parameters of the sheets and honeycomb.



Figure 3-1. Regular (solid wall) Honeycomb

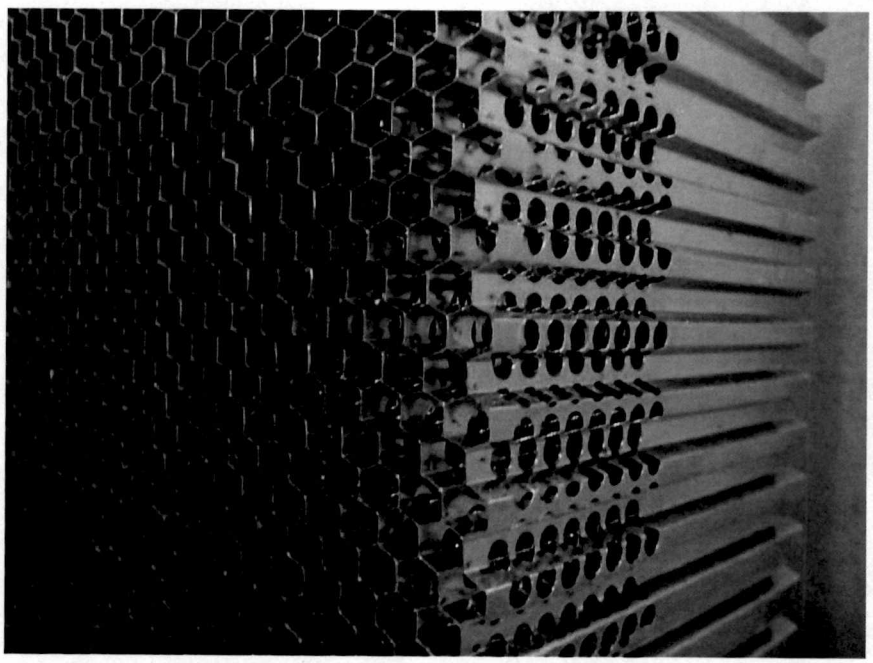


Figure 3-2. 20% Porosity Honeycomb

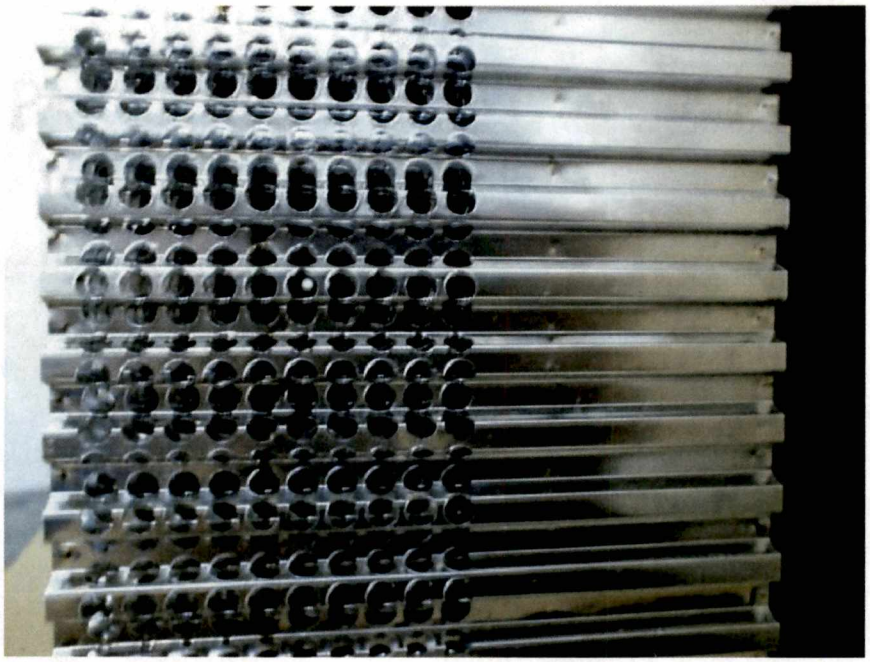


Figure 3-3. 30% Porosity Honeycomb

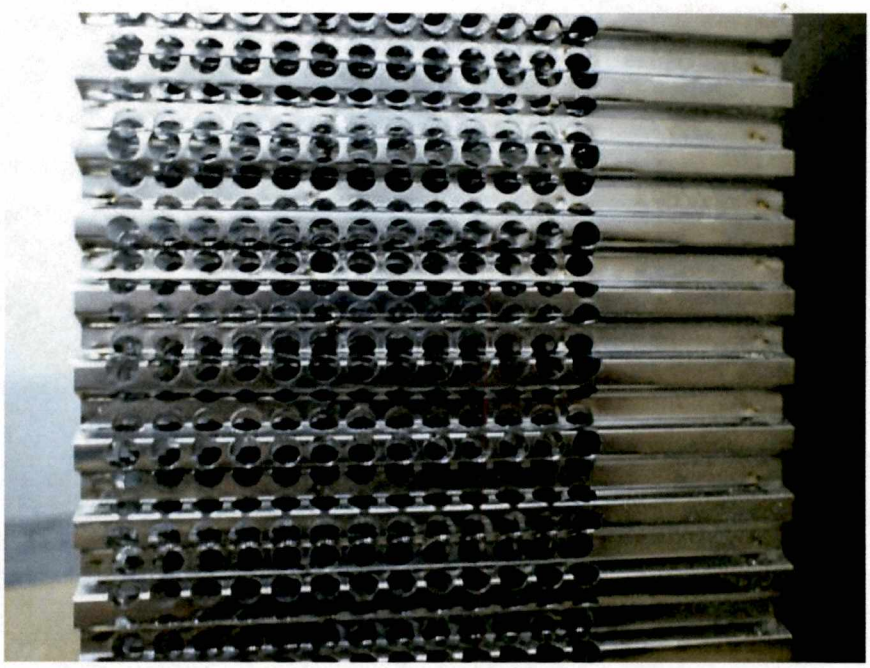


Figure 3-4. 40% Porosity Honeycomb

Table 3-1 Honeycomb Dimensions and Key Parameters

Honeycomb	Rows of Holes	Approx. Porous Area	Width (inches)	Height (inches)	Length (inches)
Regular	-	-	12	12	6
20 %	7	2" x 18"	15.5	12	6
30%	10	3" x 18"	15.5	12	6
40%	13	4" x 18"	15.5	12	6

Additional porous honeycomb design parameters are:

- 0.375 inches hex cells
- 61 sheets of 0.005 inches stainless steel was used to fabricate the porous honeycomb
- Hole diameters are all 0.25 inches
- Holes are 0.3125 inches, center- to-center.

Chapter 4

Particle Image Velocimetry Test

Experiment Objectives

Particle Image Velocimetry (PIV) was used to measure the velocity of smoke particles in the flow and then calculate vorticity and turbulence contours of the flow downstream of the honeycomb. The PIV technique also added a flow visualization element to the study. The results of the PIV test were used to determine which honeycomb performed the best at reducing turbulence generated from a cylinder placed in the wind tunnel.

Experiment Set-up and Method

PIV Set-up

The PIV test was conducted in the UTSI Low-Speed Wind Tunnel. The UTSI PIV system consists of two Continuum Nd YAG lasers, a laser controller for each laser, laser synchronizer, laser telescoping arm, analysis computer, and a PIVCAM 10-30 camera. Reference Appendix A for a description of how the PIV functions and for the PIV calibration. Figure 4-1 depicts the PIV and wind tunnel arrangement.

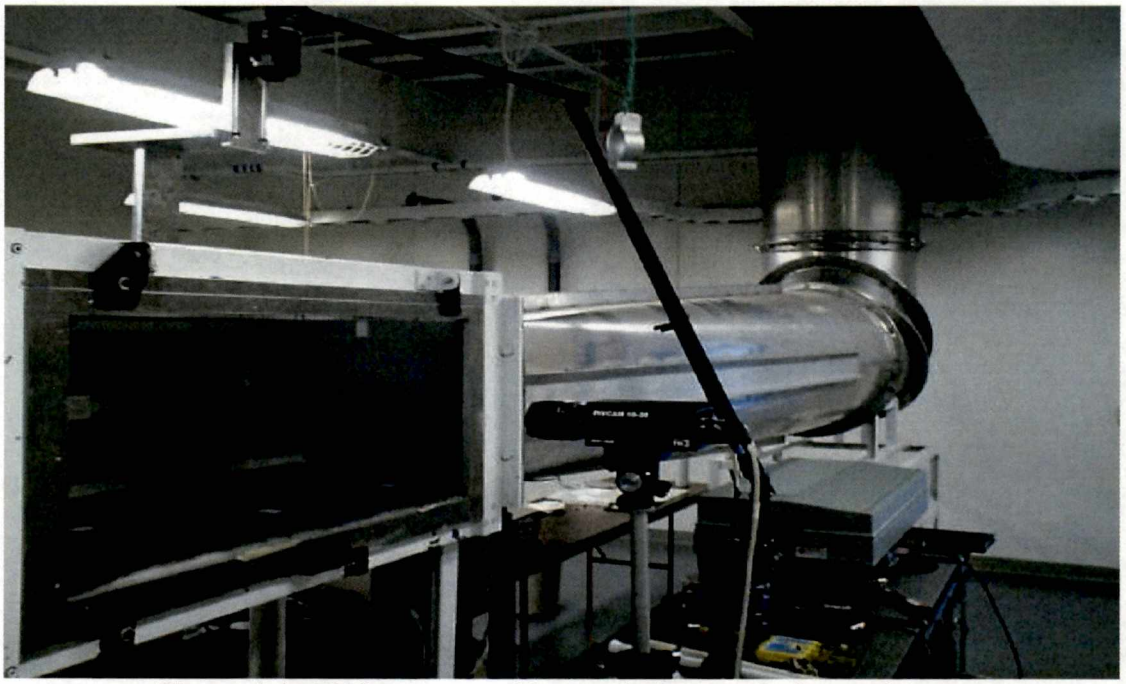


Figure 4-1. PIV camera and laser relative to wind tunnel

The best cylinder diameter and method of smoke injection for the PIV test was determined by trial and error. Cylinder sizes of 1.1, 1.9 and 3.5 inches were tested to determine which diameter developed the best turbulence structure – one that exhibited characteristics of a Karman vortex street wake. The 1.9-inch diameter pipe was selected based on its observed performance. Based on measurements from the hot film test, the cylinder Reynolds number is 55106 and the Strouhal number is 0.2 in this Reynolds number range. Chapter 5 describes the hot film test in more detail, and includes the Reynolds and Strouhal calculations. For smoke injection, the first attempts were made by injecting smoke into the cylinder and allowing smoke to escape through a slit. This approach did not work because smoke could not disperse enough to cover the plane

where the PIV camera would capture its image. The most successful approach was with an aerodynamic smoke injector inserted from the bottom of the tunnel as depicted in figure 4-2.

PIV Test Method

PIV data was collected for six test configurations as follows: a clean tunnel with no honeycomb or cylinder, cylinder with no honeycomb, cylinder with regular honeycomb,

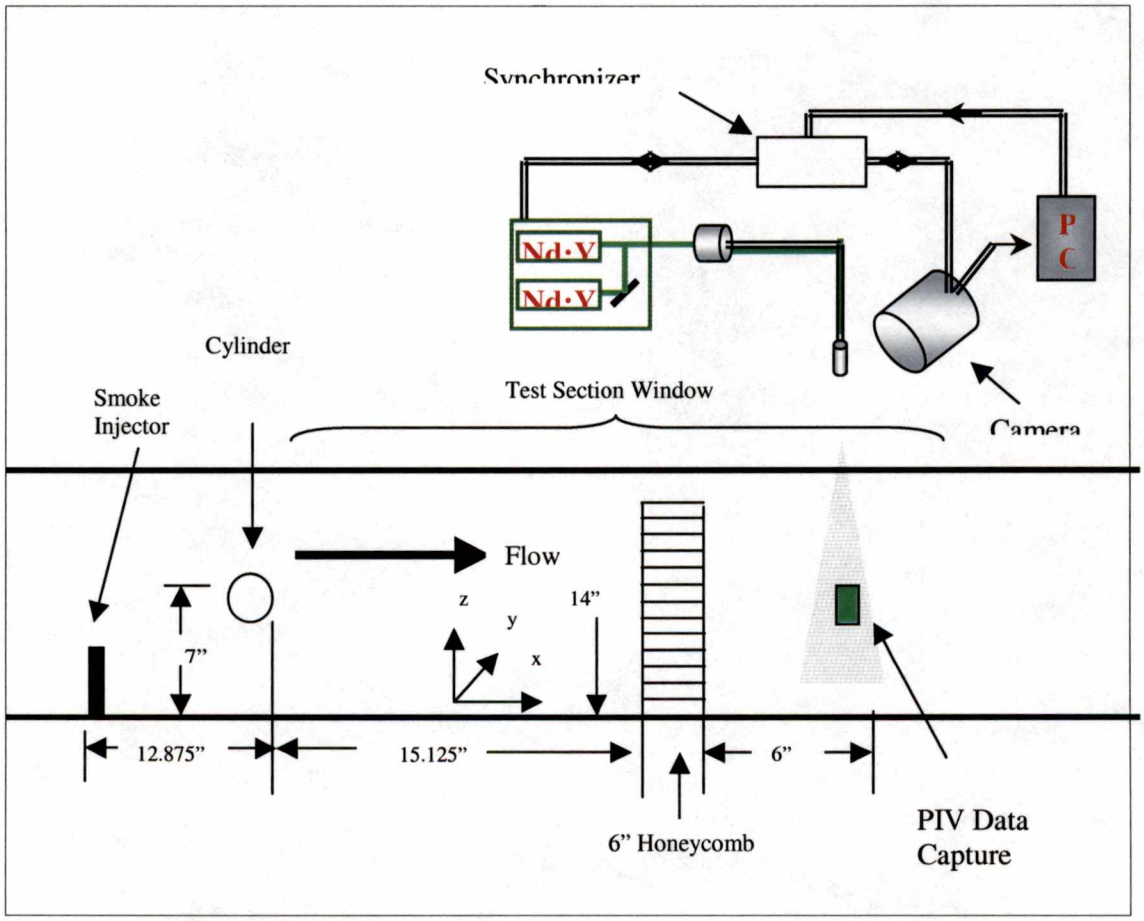


Figure 4-2. Diagram of PIV test set-up

cylinder with 20 percent porosity honeycomb, 30 percent porosity honeycomb and 40 percent porosity honeycomb. For each configuration, the PIV captured 30 data sets. A data set consists of two frames taken at 10^{-6} seconds apart. The size of the image from the PIV camera was 80 millimeters or 3.15 inches in the z-axis by 60 millimeters or 2.36 inches in the x-axis. This plane is located on the centerline of the tunnel in the y-axis. This plane is located downstream of the honeycomb. From the images, the PIV software determined velocity vectors in the x-z plane for the captured smoke particles. Figure 4-3 is the PIV laser flashing to highlight smoke particles. Figure 4-4 depicts a picture of smoke particles captured by the PIV system.

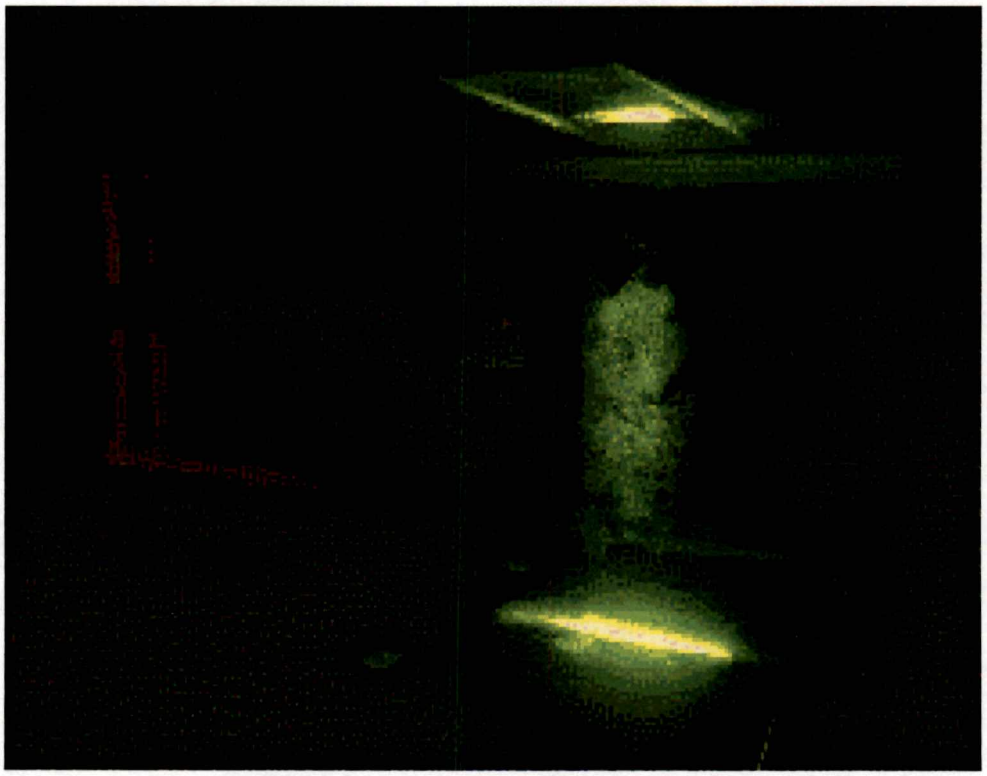


Figure 4-3. PIV Laser Flash

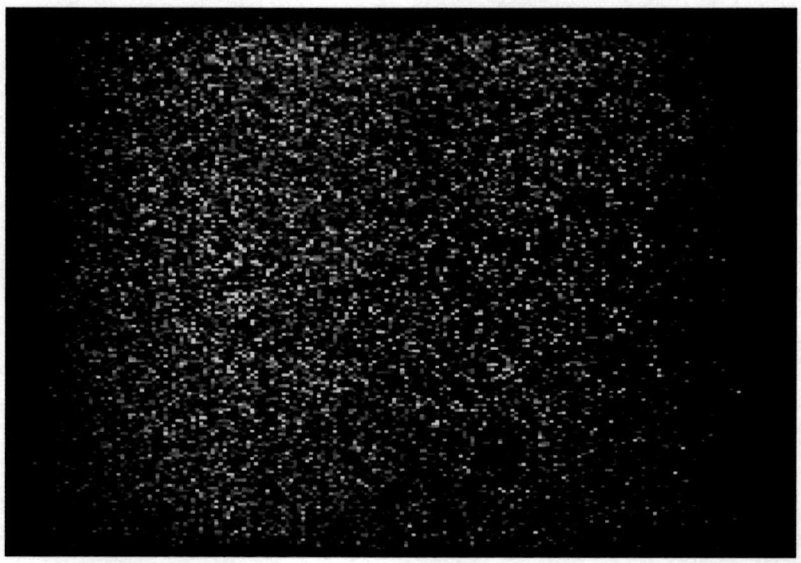


Figure 4-4. PIV Picture of Smoke Particles

Analysis Approach

From velocity vector data, Tecplot was used to calculate vorticity and turbulence intensity contours in the x-z plane. Vorticity is a measure of the rotation of the flow induced by viscous effects and can be used to describe fluid motion. Vorticity is defined as follows:

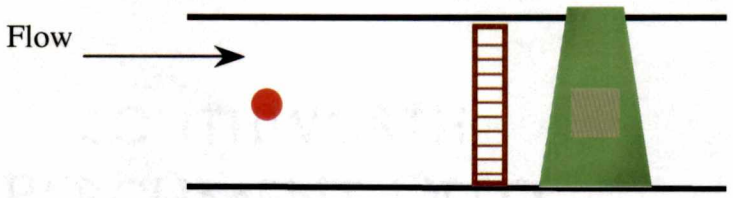
$\overline{\zeta} = \nabla \times \overline{V}$.

The vorticity of a fluid element is associated with its angular deformation. For example, an inviscid or irrotational flow has zero vorticity, $\overline{\zeta} = \nabla \times \overline{V} = 0$ [2. Munson, p314]. For flow quality considerations, very low vorticity is desirable.

Results and Analysis

Figure 4-5 depicts turbulence intensity contours in the x-z plane from the PIV test. The image at the top of the contour illustrates flow over the cylinder, through the honeycomb and then through PIV laser plane. The clean tunnel is depicted in the upper left and the cylinder only contour is in the upper middle. The addition of the cylinder raised the turbulence intensity from 5-to-11 percent to 16-to-25 percent. The regular honeycomb is depicted in the upper right and reduces turbulence intensity to below 16 percent with a large section at 5 percent. The bottom right contour depicts the 20 percent porosity honeycomb, which shows an increased section in the 5 percent range in the lower half of the contour. The bottom center contour is the 30 percent porosity honeycomb, the bottom left is the 40 percent porosity honeycomb, and both show a definite improvement over the regular and 20 percent porosity honeycomb.

Figure 4-6 depicts instantaneous vorticity contours in the same order as the turbulence intensity contours. In general, the same trend as the turbulence intensity contours is present in the vorticity contours. The 30 percent porosity appears to perform the best in the vorticity contours. PIV results in the turbulence intensity and vorticity contours indicates that porous honeycomb may be more effective than regular honeycomb at reducing turbulence.



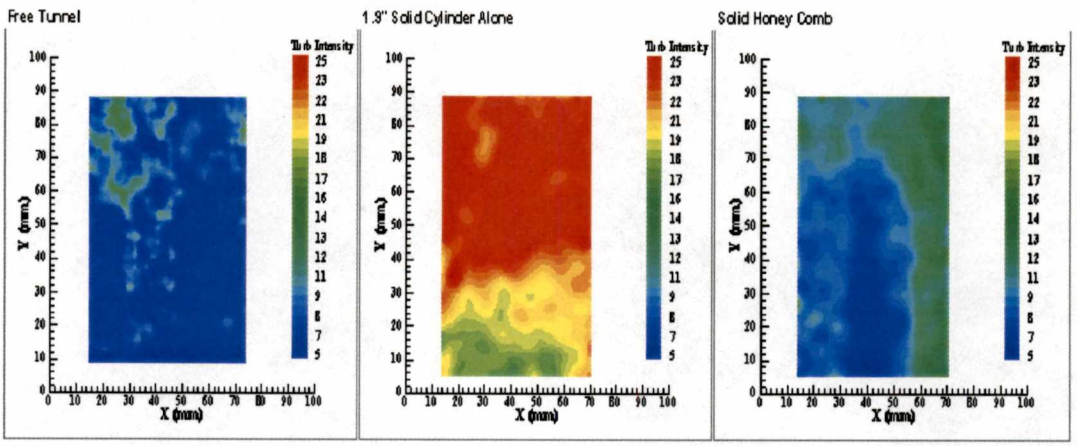


Figure 4-5. PIV Turbulent Intensity Contours

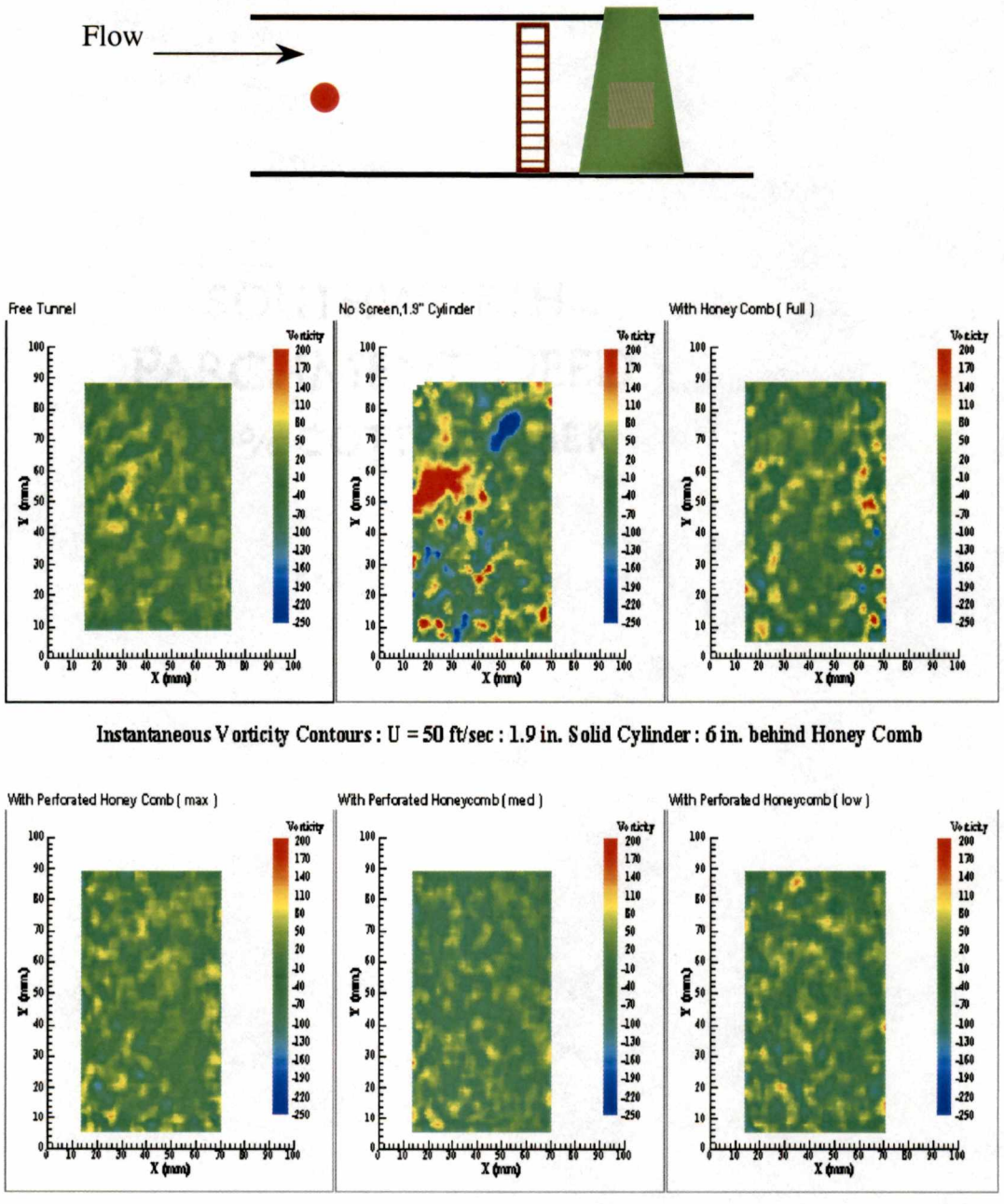


Figure 4-6. PIV Instantaneous Vorticity Contours

Chapter 5

Velocity Field Measurements Using Hot Film Sensors

Experiment Objectives

The objective of the velocity flow field measurement test was to make detailed quantitative measurements of the flow fields in the wake of the cylinder in order to quantify the effectiveness of each honeycomb model at reducing turbulence generated by the cylinder. The measured effectiveness of reducing turbulence for each honeycomb would then be used in a comparison analysis to determine how effective porous honeycomb is at turbulence reduction.

Experiment Set-up, Method, and Analysis Approach

Experiment Set-up

The hot-film test used the same wind tunnel as PIV test. The UTSI IFA 300 Thermal Anemometer System was used to collect and process the data. Two sensors were used to measure the flow velocity downstream of each honeycomb model. Details on the calibration of the hot film sensors are available in Appendix B.

The set-up for the hot film test was identical to the PIV test, Figure 4-2, except for the addition of two hot-film sensors downstream of the same honeycomb models. Figure 5-1 diagrams the location of the test models and the test support equipment for the hot film

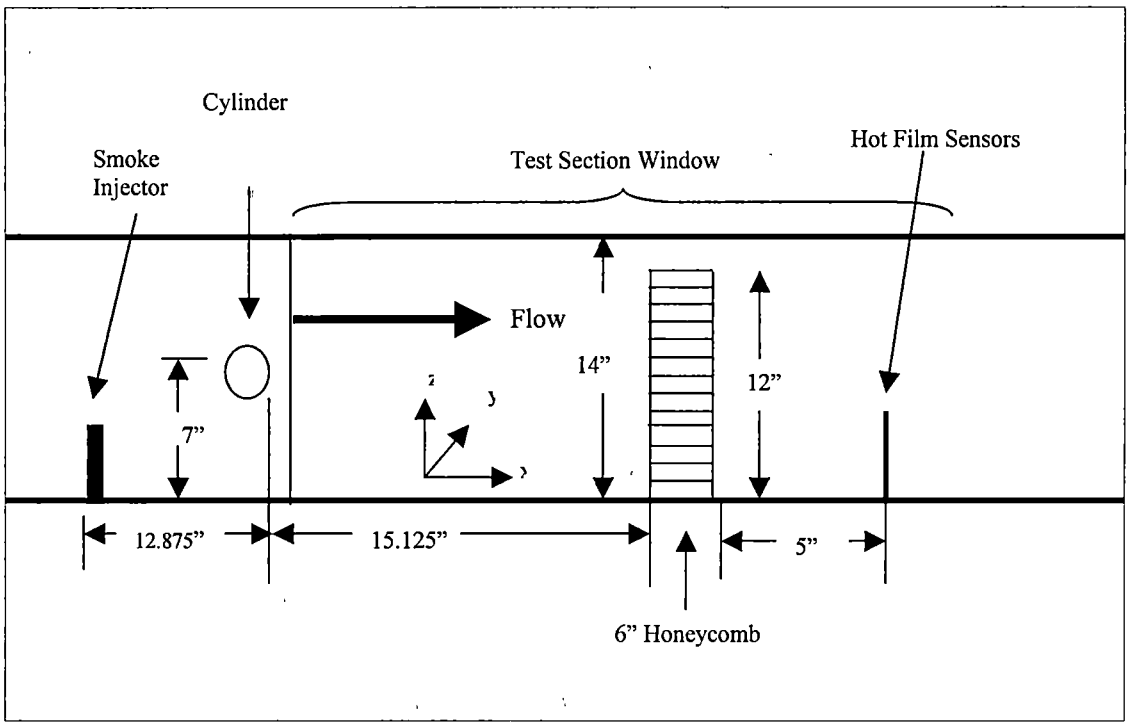


Figure 5-1. Diagram of Hot Film Test

sensors. Figure 5-2 shows the cylinder upstream of the regular honeycomb. The dimensions of the test cell window section are 14 inches in the z-axis, 20 inches in the y-axis and 36 inches in the x-axis. The cylinder was placed mid-level in the tunnel, which corresponds to 7 inches from the bottom of the tunnel. Two hot-film sensors were placed 5 inches downstream of the honeycomb and 5/8 of an inch apart in the y-axis. Sensor 4 was 6.5 inches from the bottom, in the z-axis, of the tunnel and sensor 5 was 8.5 inches from the bottom. The height of the sensors corresponds to the top and bottom of the cylinder. The hot film sensors were oriented such that the downstream flow axis would correspond to a normal velocity across the sensor wire.

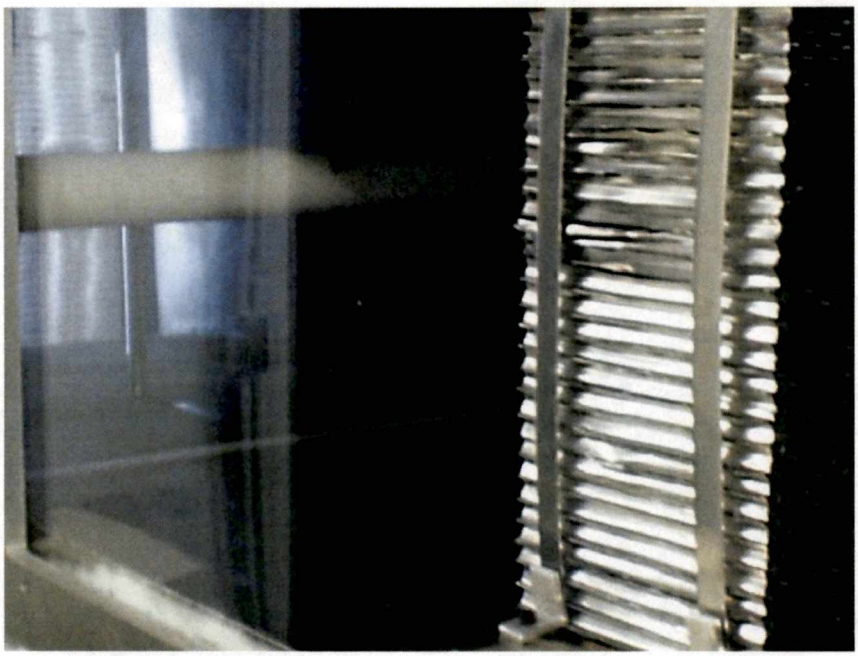


Figure 5-2. Test Section

Reference Figure B-1 in the Hot Film Calibration Appendix, Appendix B, for an illustration. The hot-film sensors measured a clean tunnel velocity of 55 ft/sec and this tunnel velocity was used for all test configurations. As in the PIV test set-up, the 1.9-inch diameter cylinder was used to generate large-scale turbulence that had characteristics of an oscillating Karman vortex street wake. Reynolds number (Re) and Strouhal (St) number provide non-dimensional characteristics to characterize this type of flow. Reynolds and Strouhal number are expressed as follows:

$$\mathrm{Re}_d = \frac{\rho U_\infty d}{\mu} = \frac{U_\infty d}{\nu}$$

$$\mathrm{St} = \frac{fd}{U_\infty}$$

where

f = frequency

d = 1.9 in or 0.158 ft

$\rho = 2.373 * 10^{-3}$ slug/ft^3

$\mu = 3.75 * 10^{-7}$ lb sec/ft^2.

The Reynolds number based on a clean tunnel velocity of 55 ft/sec and the cylinder diameter of 1.9 inches is 55,106 and the Strouhal number in this Reynolds number range is 0.2. This Strouhal number predicts an oscillating flow about the cylinder at a frequency of 69.83 Hz.

Experiment Method

Hot-film data was collected for six test configurations which included: a clean tunnel with no honeycomb or cylinder, cylinder with no honeycomb, cylinder with regular honeycomb, cylinder with 20 percent porosity honeycomb, 30 percent porosity honeycomb and 40 percent porosity honeycomb. For each configuration, eight data runs were performed with the IFA 300 set to collect at 5000 data points per second and a data collection time period of 3.2766 seconds, which resulted in 16384 data points. Each data point contained time, velocity, frequency, and amplitude results. For the analysis of the velocity and turbulence intensity, the mean velocity, velocity variance, standard deviation, instantaneous turbulence intensity, percent turbulence intensity and mean turbulence intensity was calculated and used for comparison analysis. For the frequency spectrum analysis, the frequency and amplitude were compared to determine which honeycomb had the best damping performance.

Analysis Approach

A velocity trace with time can be decomposed into a mean velocity component, $\overline{U}$ and a fluctuating velocity component, U_i' [2. Munson, p 475] . This velocity decomposition can be expressed as:

$$U_i = \overline{U} + U_i'$$

The mean velocity component is a constant velocity upon which the fluctuating velocity component is equally distributed on each side of the mean and is expressed in the following equation:

$$\overline{U} = (1/\mathrm{N}) \sum_{i=1}^{N} U_i$$

where N is the number of data samples.

Velocity variance is the sum of the squares of the fluctuating velocity component divided by the number of data points. When comparing the performance of different honeycomb samples, the lowest value of velocity variance is most desirable because it is interpreted to imply the smallest velocity fluctuations about the mean. Velocity variance is expressed as:

$$\overline{U'} = (1/N) \sum_{i=1}^{N} (U')^2 = (1/N) \sum_{i=1}^{N} \left(\overline{U} - U_i\right)^2$$

Standard deviation is the square root of the velocity variance and is expressed as:

$$\tau = \sqrt{\overline{U'}}$$

Standard deviation is used to define and calculate the level of turbulence or turbulence intensity in the velocity trace with time. Percent turbulence intensity [2. Munson, p 476] is expressed as follows:

$$\%TI = (\tau / \overline{U}) * 100$$

The instantaneous turbulence intensity is the value of turbulence associated with a velocity component at an instant in time and is expressed as follows [8. McKeage, p 27]:

$$TI = \sqrt{(\overline{U} - U_i)^2} \Big/ \overline{U}$$

Mean turbulence intensity provides a good reference value when graphing instantaneous turbulence intensity and is expressed as:

$$MTI = (\sum_{i=1}^{N} TI_i) \Big/ N$$

Percent turbulence intensity provides a cumulative value of turbulence where as instantaneous is a snap shot of turbulence in time. As with velocity variance, when comparing the performance of different honeycomb samples, the lowest value of percent turbulence intensity and mean turbulence intensity is most desirable.

Results and Analysis

Velocity Field Results

The results presented in the Figures 5-3 through 5-14 were calculated from the data based on the equations for velocity variance, standard deviation and percent turbulence intensity. The log of the mean velocity was used to accommodate the scale of the vertical axis. The appendices contain graphs of velocity, mean velocity, instantaneous turbulence intensity and mean turbulence intensity for all eight data runs on each of the six test configurations.

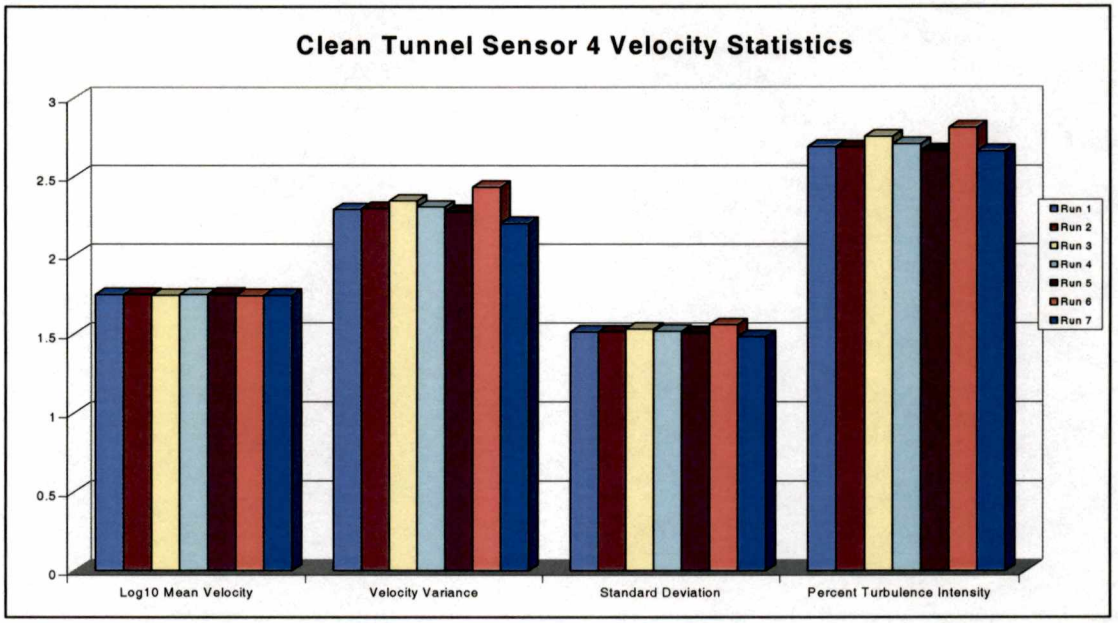


Figure 5-3. Clean Tunnel Sensor 4 Velocity Statistics

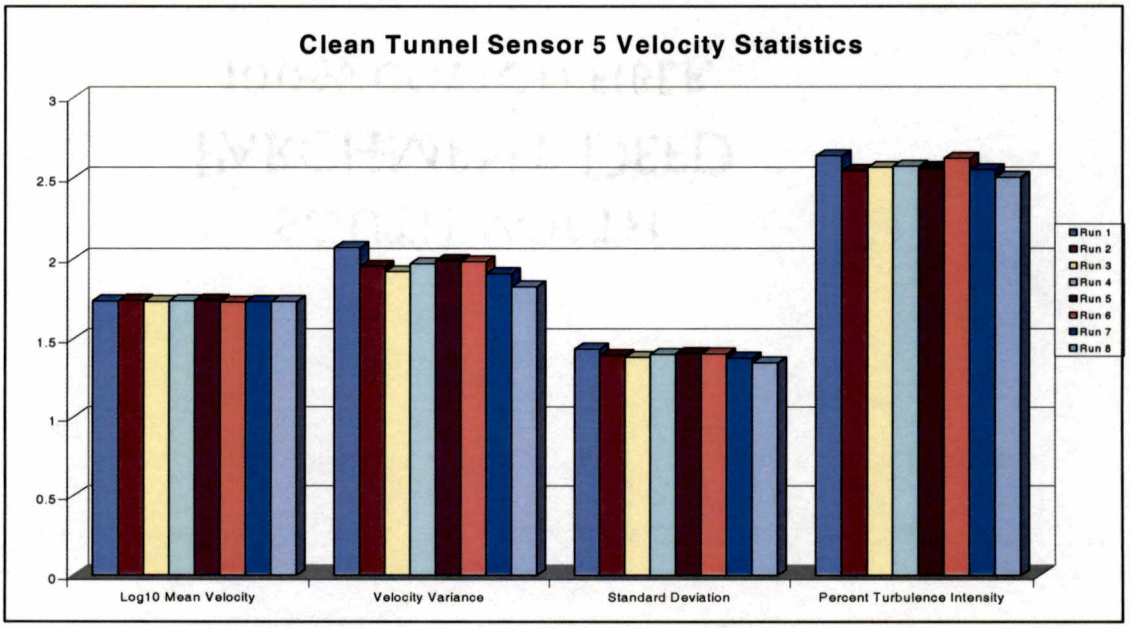


Figure 5-4. Clean Tunnel Sensor 5 Velocity Statistics

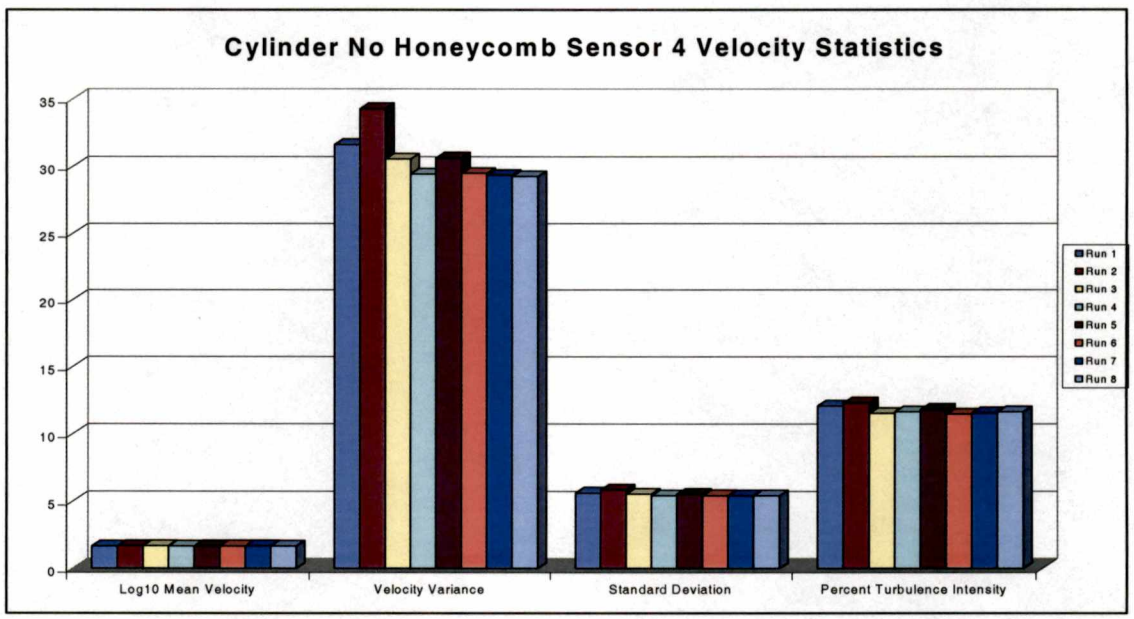


Figure 5-5. Cylinder No Honeycomb Sensor 4 Velocity Statistics

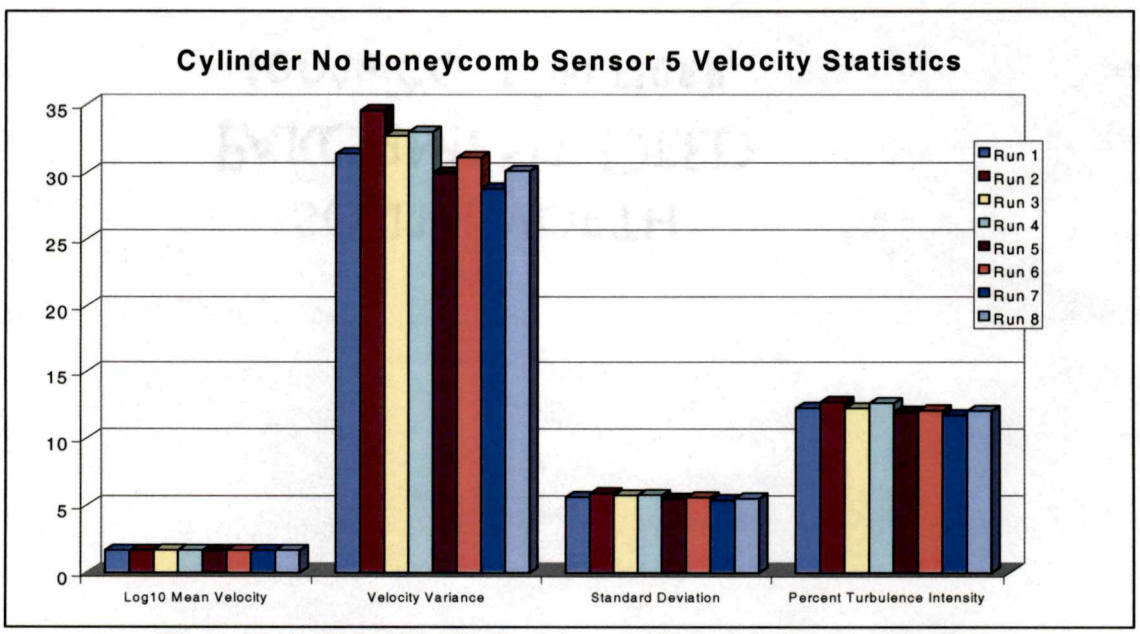


Figure 5-6. Cylinder No Honeycomb Sensor 5 Velocity Statistics

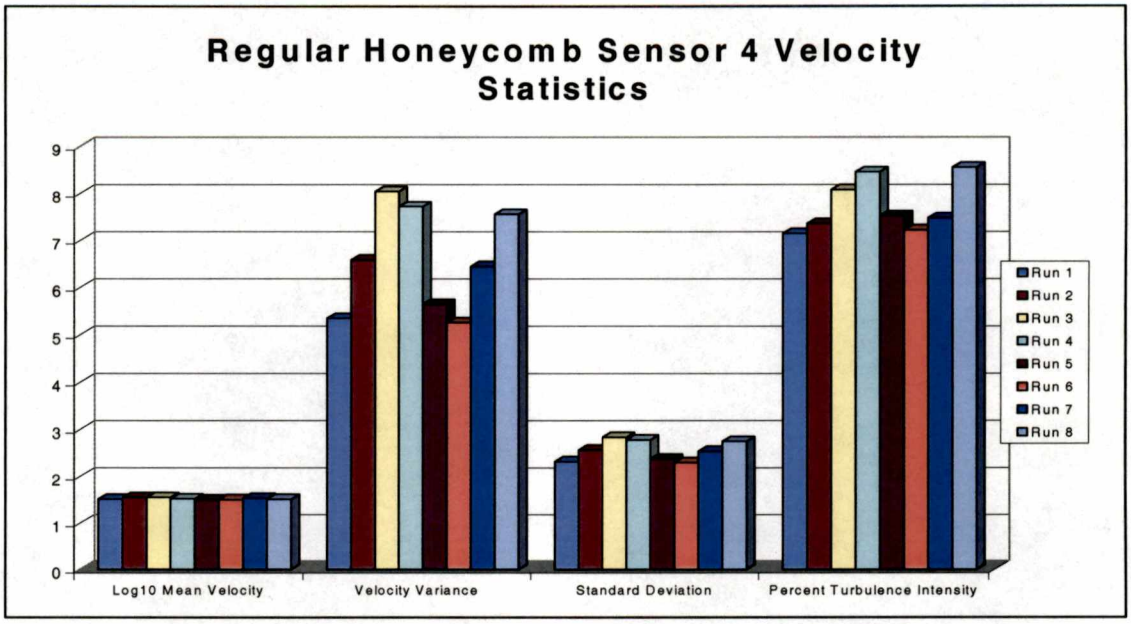


Figure 5-7. Regular Honeycomb Sensor 4 Velocity Statistics

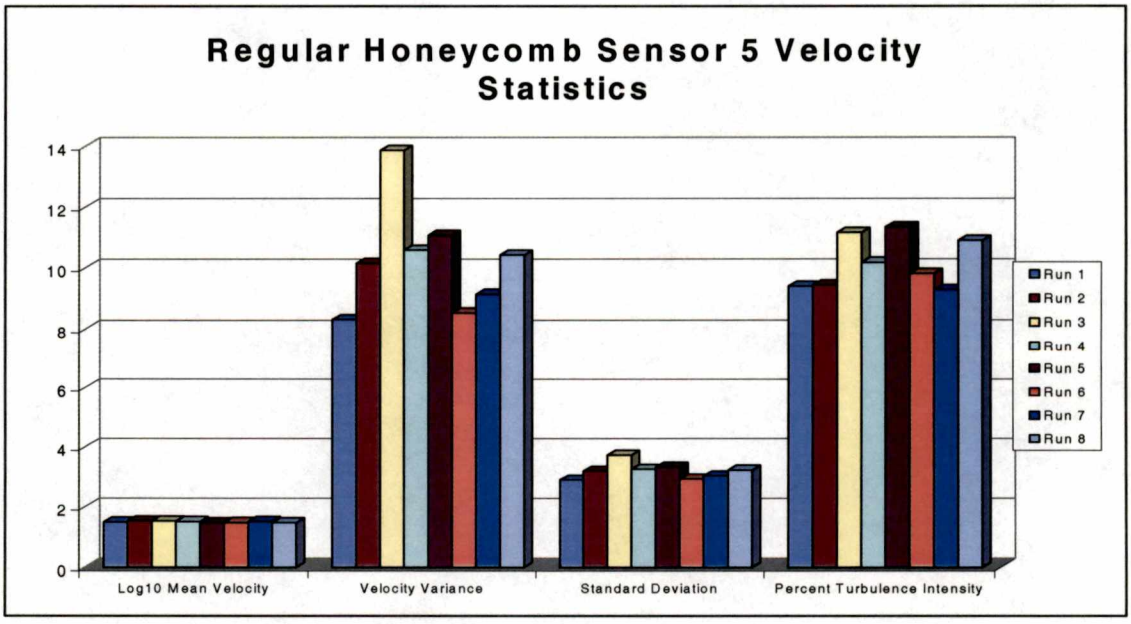


Figure 5-8. Regular Honeycomb Sensor 5 Velocity Statistics

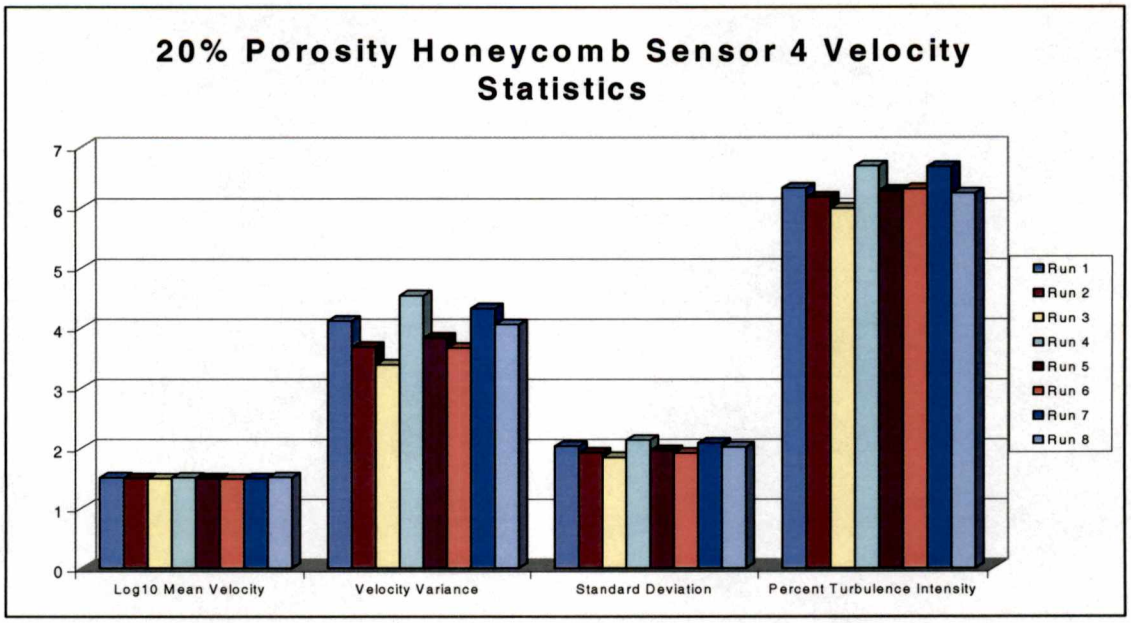


Figure 5-9. 20% Porosity Honeycomb Sensor 4 Velocity Statistics

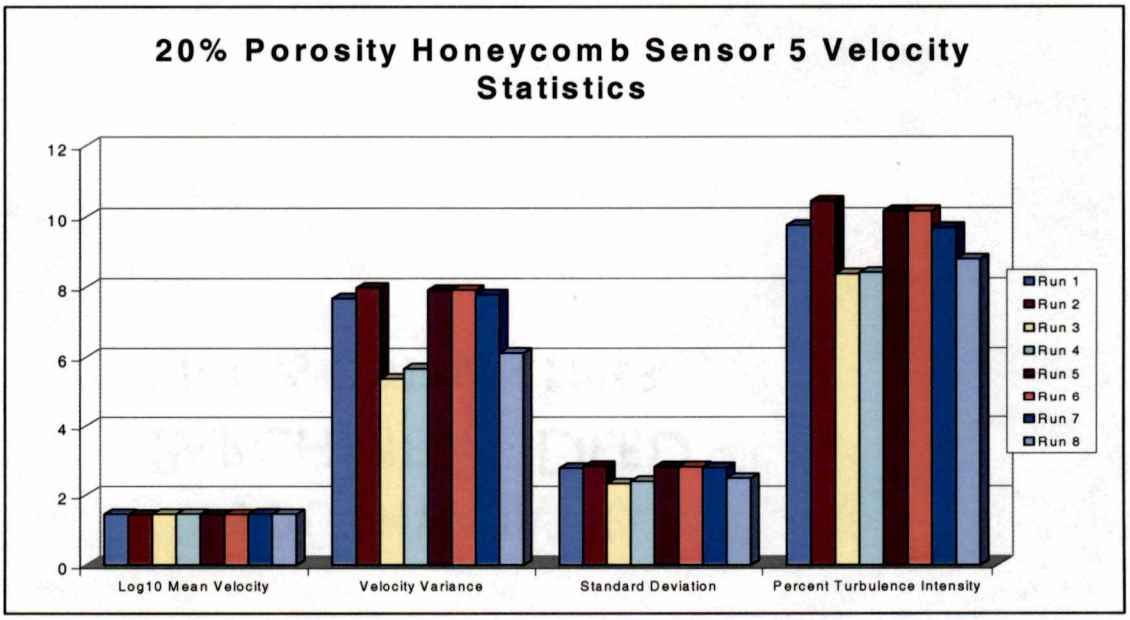


Figure 5-10. 20% Porosity Honeycomb Sensor 5 Velocity Statistics

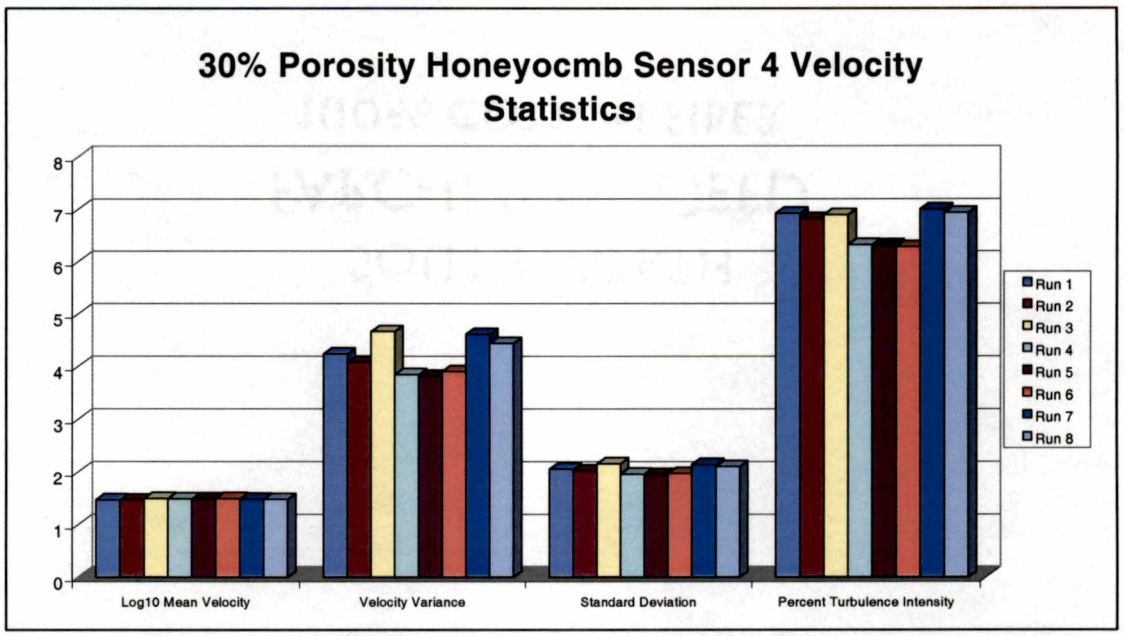


Figure 5-11. 30% Porosity Honeycomb Sensor 4 Velocity Statistics

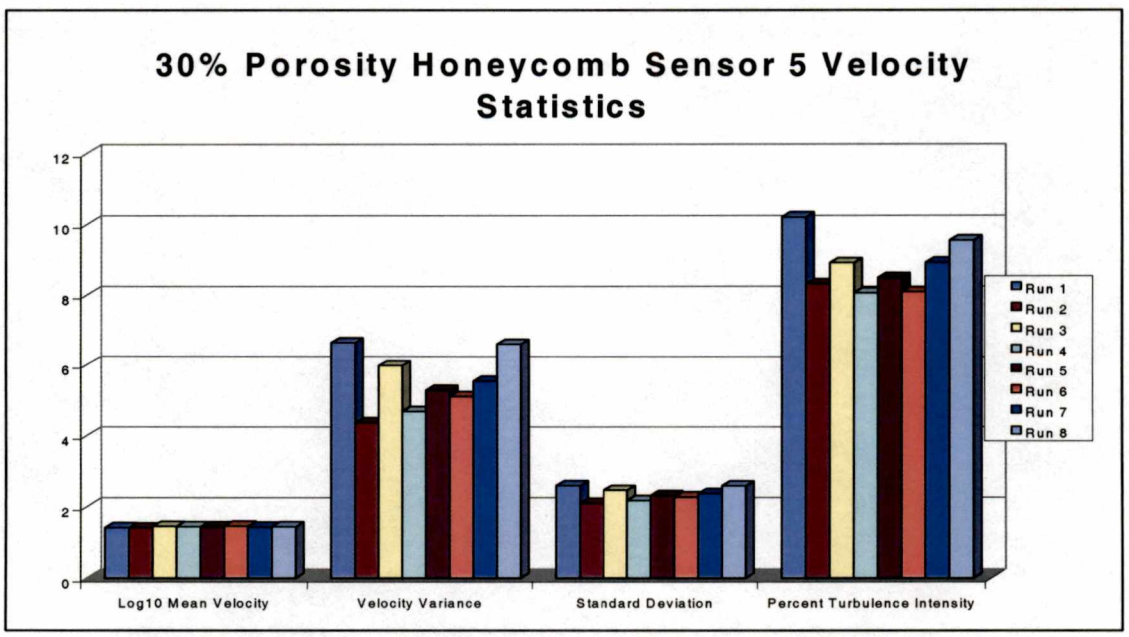


Figure 5-12. 30% Porosity Honeycomb Sensor 5 Velocity Statistics

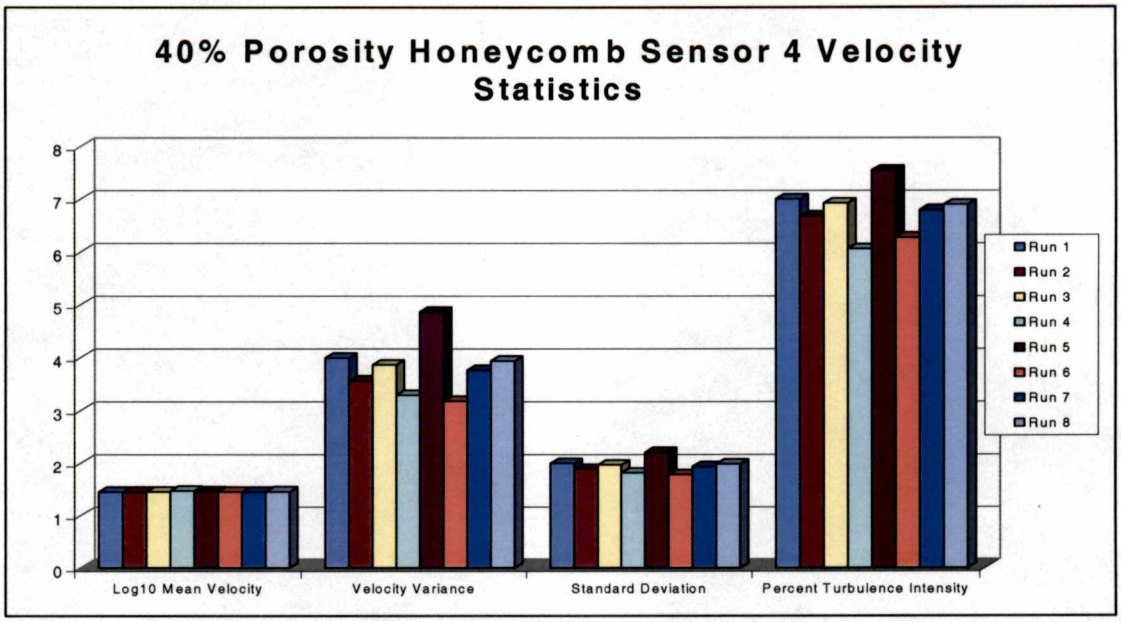


Figure 5-13. 40% Porosity Honeycomb Sensor 4 Velocity Statistics

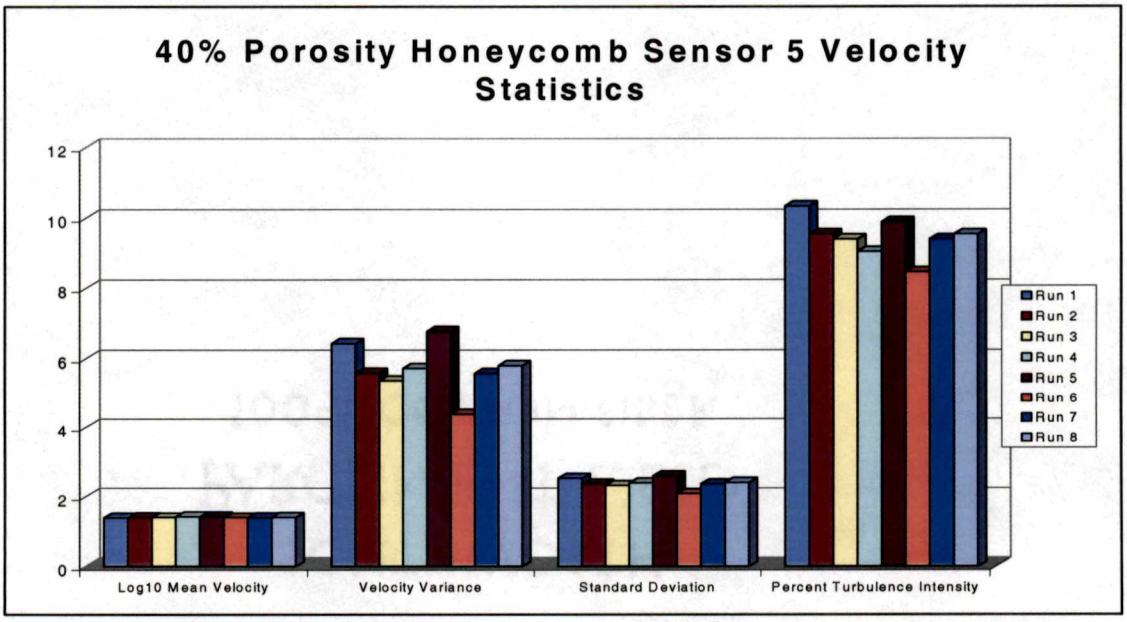


Figure 5-14. 40% Porosity Honeycomb Sensor 5 Velocity Statistics

Velocity Field Analysis

The analysis of the velocity and turbulence intensity data for the test configurations will start with a comparison of the clean tunnel configuration to the tunnel and cylinder configuration, without any honeycomb installed. Next, the performance of each honeycomb will be compared to the cylinder with no honeycomb to illustrate how each dampens the turbulence created by the cylinder. The majority of the following analysis will focus on the results from sensor 4. This is due to the suspected wake generated from flow over the top of the honeycomb interfering with sensor 5. The height of the honeycomb is 12 inches and the height of the tunnel is 14 inches leaving a 2-inch gap for air to flow over the top of the honeycomb. This suspicion is quantified and illustrated in Figure 5-15.

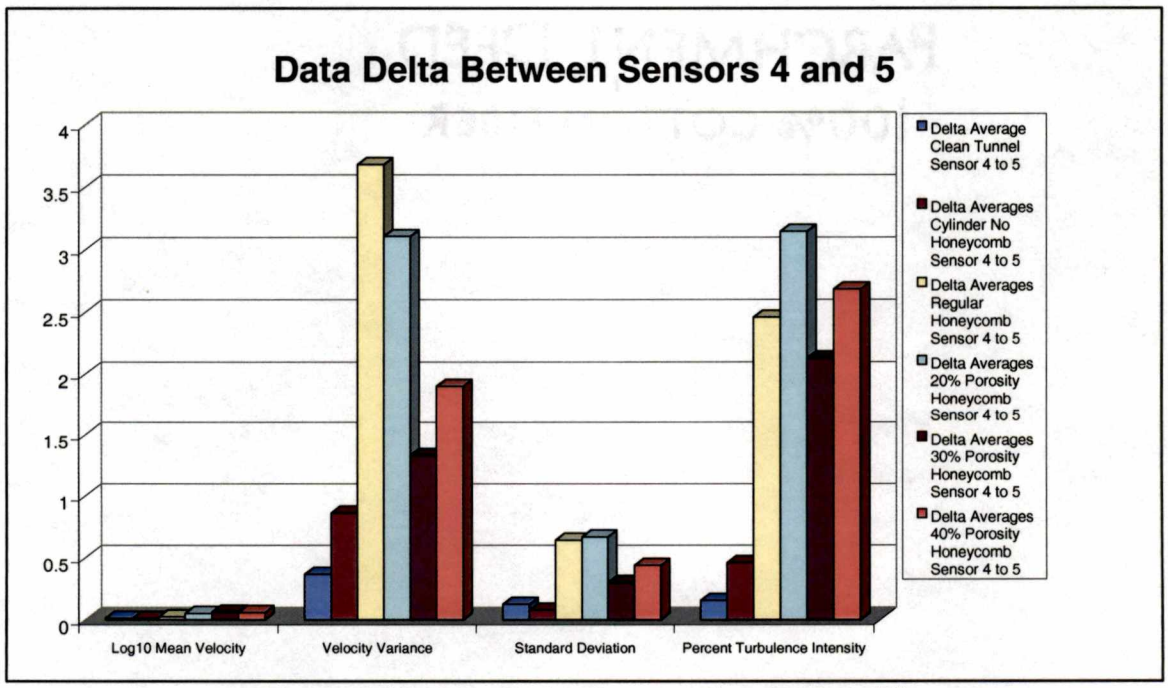


Figure 5-15. Data Delta Between Sensors 4 and 5

This can also be observed by comparing the charts in Figures 5-3 through 5-14 and noting that for all eight runs for the clean tunnel configuration and the cylinder only configuration, the data from sensors 4 and 5 had relatively the same values. With the introduction of honeycomb, sensor 5 experienced a noticeable difference from sensor 4 in all eight data runs for the honeycomb configurations. For example, Figure 5-15 illustrates that the delta between sensor 4 and 5 for turbulence intensity for the cylinder only is 0.457 and the delta in turbulence intensity for the regular honeycomb configuration is 2.456.

Comparison of Clean Tunnel to Cylinder No Honeycomb

Selecting data run 4 from Figure 5-3 as a representative of the clean tunnel configuration and data run 5 from Figure 5-5 as a representative of the cylinder no honeycomb configuration shows the dramatic increase in velocity variance and turbulence due to the introduction of the 1.9-inch cylinder. Recall that the purpose of the cylinder was to generate turbulence and then measure the effectiveness of each honeycomb at turbulence reduction. The velocity trace with time for the clean tunnel configuration is depicted in Figure 5-16 and the velocity trace with time for the cylinder no honeycomb configuration is depicted in Figure 5-17. From Figure 5-3, the clean tunnel velocity variance for data run 4 is 2.30 and the cylinder no honeycomb velocity variance from Figure 5-5 data run 5 is 30.65. This is a dramatic increase in velocity variance. Comparing Figures 5-18 and 5-19 also illustrates a significant increase from 0.022 time mean turbulence intensity for the clean tunnel to 0.092 time mean turbulence intensity for the cylinder no honeycomb configuration.

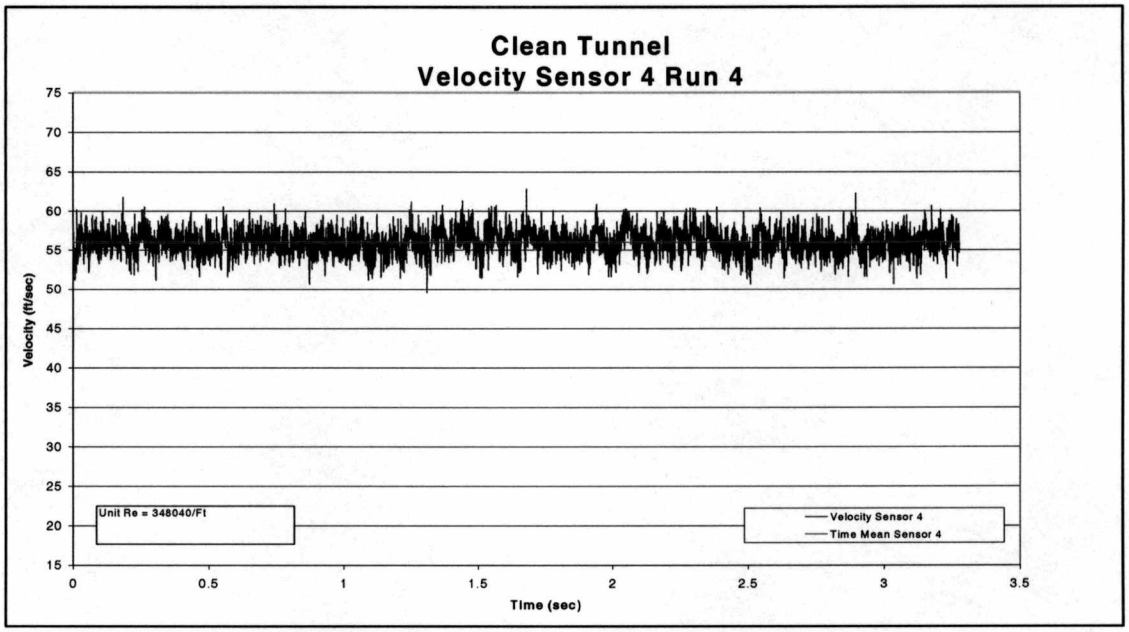


Figure 5-16. Clean Tunnel Velocity Sensor 4 Run 4

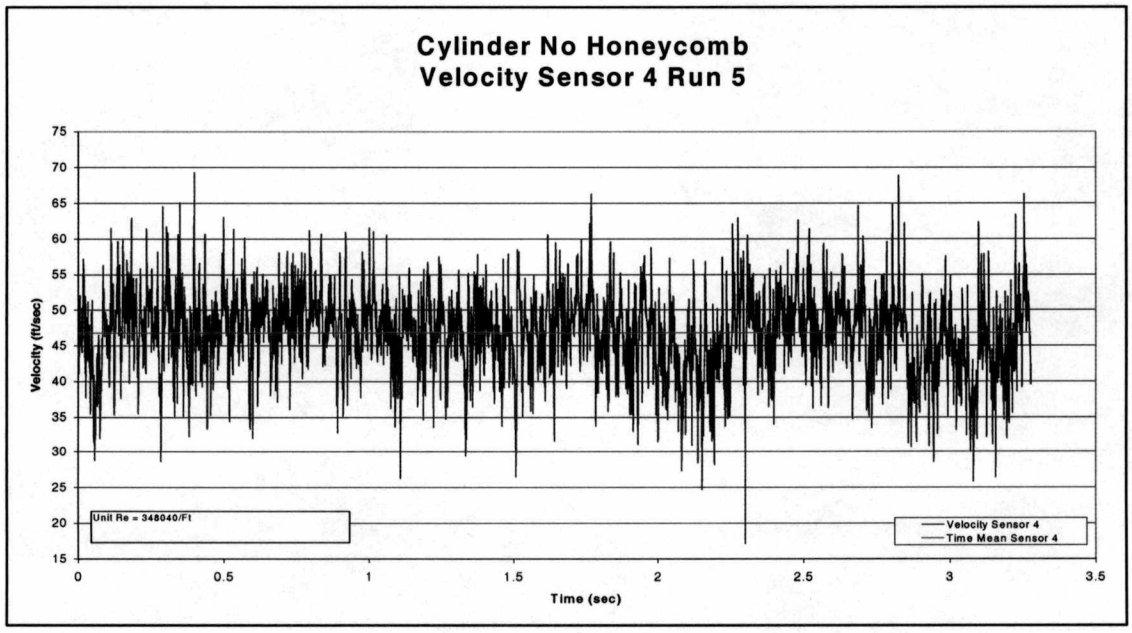


Figure 5-17. Cylinder No Honeycomb Velocity Sensor 4 Run 5

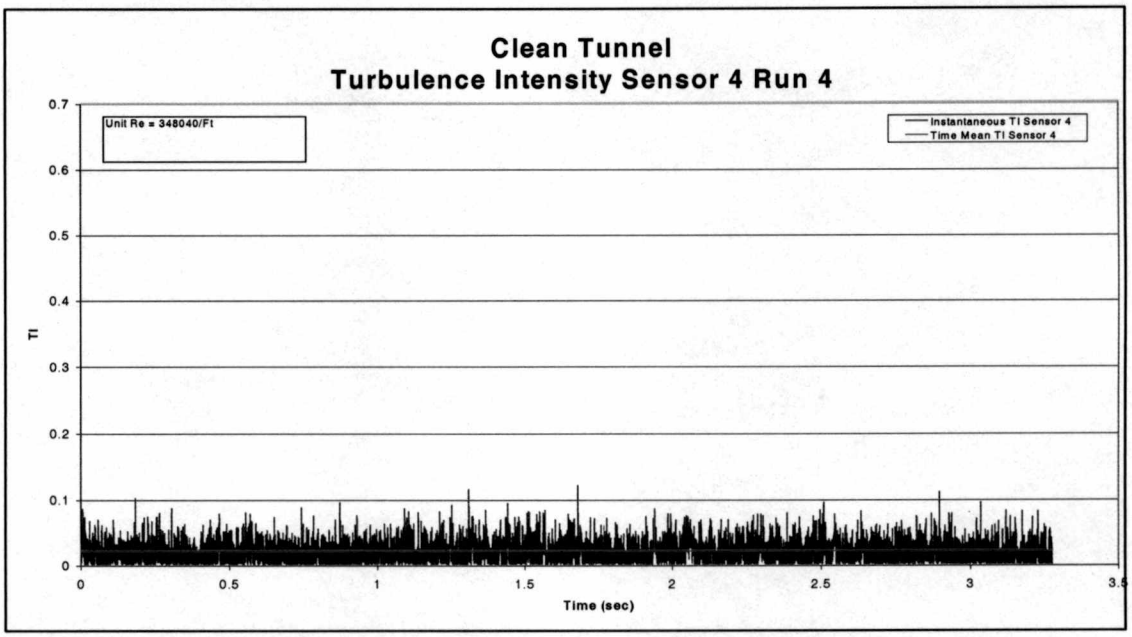


Figure 5-18. Clean Tunnel Turbulence Intensity Sensor 4 Run 4

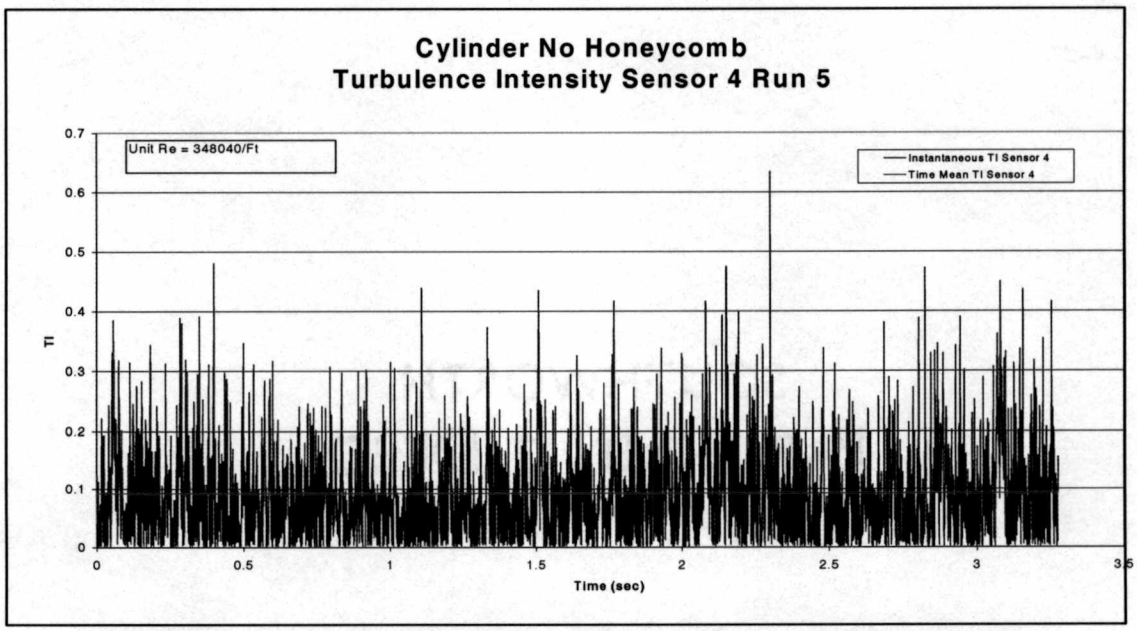


Figure 5-19. Cylinder No Honeycomb Turbulence Intensity Sensor 4 Run 5

Comparison of Cylinder No Honeycomb to Regular Honeycomb

The comparison of the cylinder with no honeycomb to the regular honeycomb begins by selecting data run 2 from Figure 5-7 as representative of the regular honeycomb configuration and comparing it to the same cylinder only data run (data run 5). Comparing the cylinder no honeycomb velocity trace in Figure 5-20 and a cylinder no honeycomb velocity variance of 30.65 from Figure 5-5 to the regular honeycomb velocity trace also in Figure 5-20 and a velocity variance of 6.44 from Figure 5-7 demonstrates the effectiveness of traditional honeycomb at reducing the fluctuating velocity components. Comparing the cylinder no honeycomb mean turbulence intensity of 0.092 from Figure 5-21 to the regular honeycomb mean turbulence intensity of 0.060 also from Figure 5-21, the regular honeycomb reduces turbulence intensity by 0.032. This demonstrates the effectiveness of regular honeycomb at reducing mean turbulence intensity.

Comparison of Cylinder No Honeycomb to 20% Porosity Honeycomb

The comparison of the cylinder no honeycomb configuration to the 20 percent porosity honeycomb is conducted by selecting data run 8 from Figure 5-9 as representative of the 20 percent porosity honeycomb configuration and comparing it to data run 5 from the cylinder only configuration. Comparing the cylinder no honeycomb velocity trace in Figure 5-22 and a cylinder no honeycomb velocity variance of 30.65 to the 20 percent porosity honeycomb velocity trace also in Figure 5-22 and a velocity variance of 4.06 from Figure 5-9 to again demonstrates the effectiveness honeycomb and a noticeable improvement from the regular honeycomb

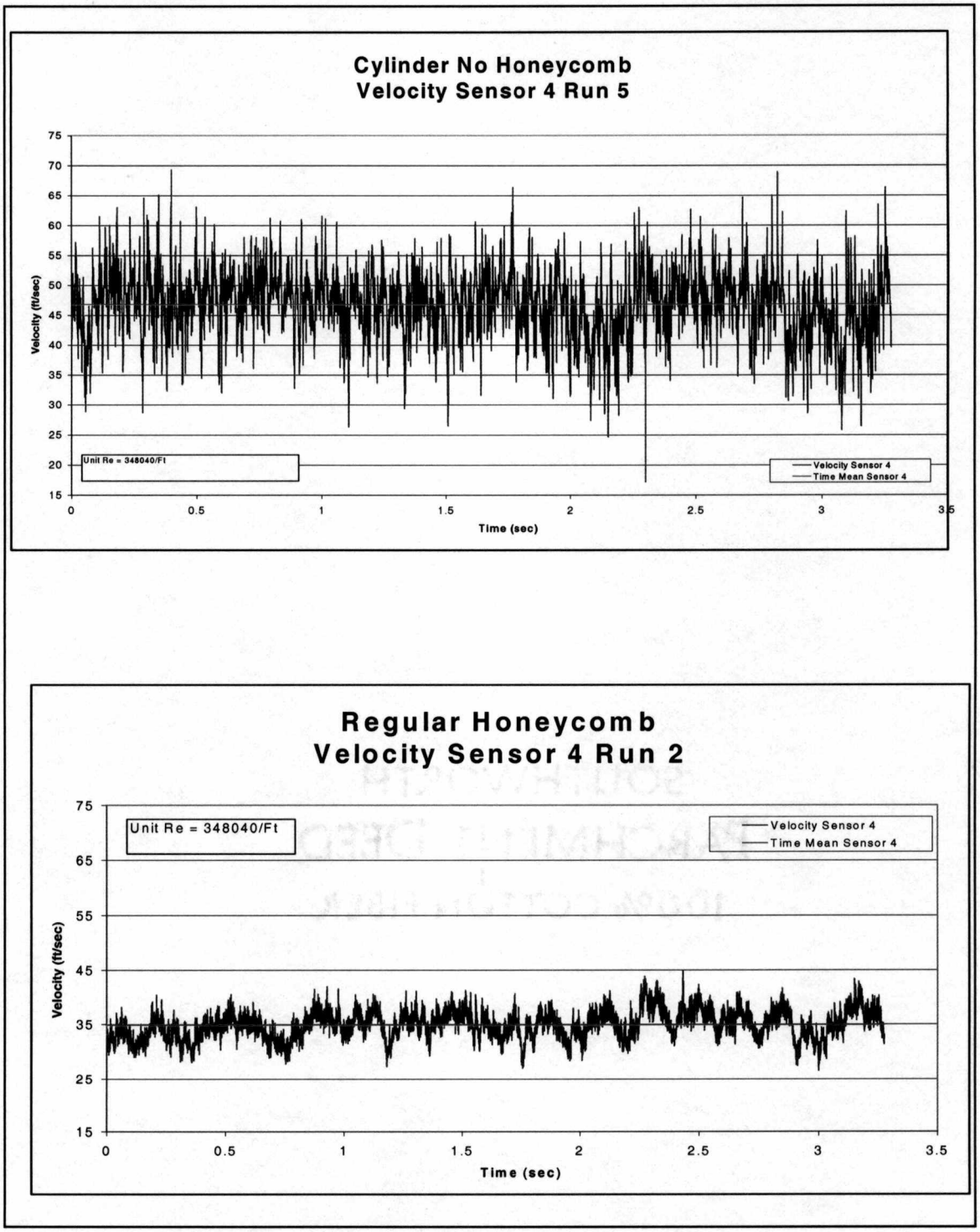


Figure 5-20. Comparison of Cylinder No Honeycomb to Regular Honeycomb Velocity

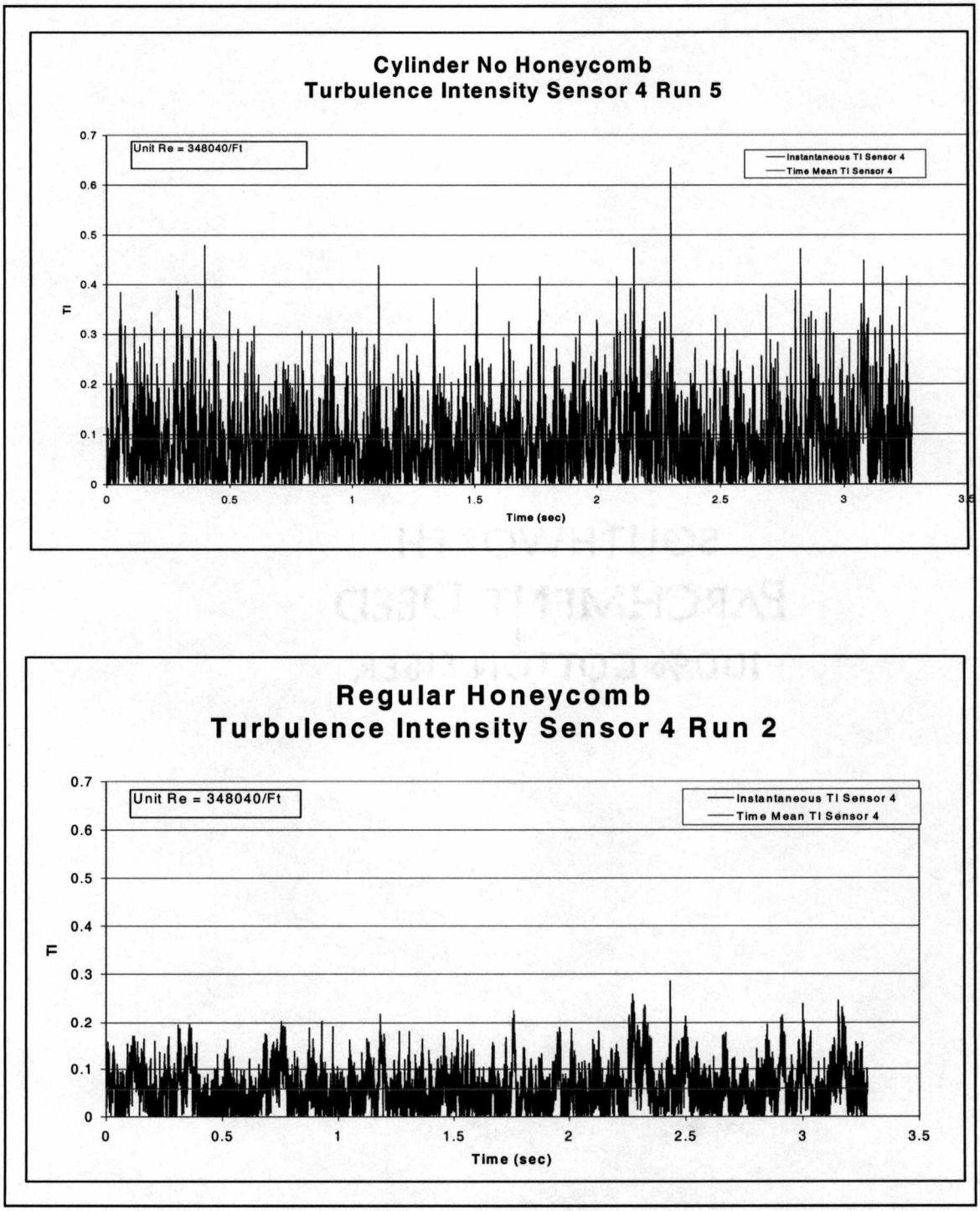


Figure 5-21. Comparison of Cylinder No Honeycomb to Regular Honeycomb Turbulence Intensity

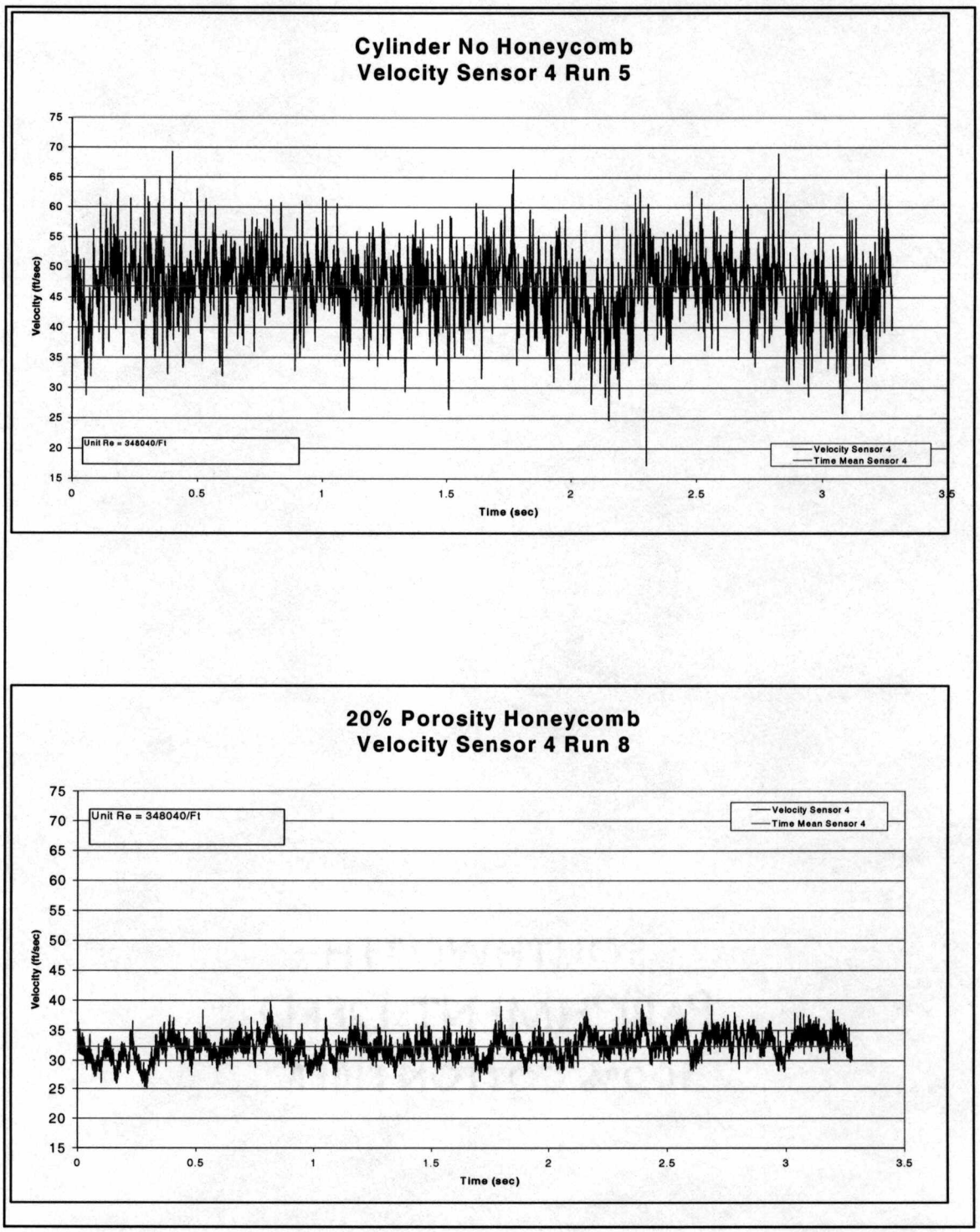


Figure 5-22. Comparison of Cylinder No Honeycomb to 20% Porosity Honeycomb Velocity

(6.44 velocity variance) at reducing the fluctuating velocity components. Comparing the cylinder no honeycomb mean turbulence intensity of 0.092 from Figure 5-23 to the 20 percent porosity honeycomb mean turbulence intensity of 0.050 also from Figure 5-23 again demonstrates the effectiveness of honeycomb at reducing mean turbulence intensity.

Comparison of Cylinder No Honeycomb to 30% Porosity Honeycomb

Comparison of the cylinder no honeycomb configuration to the 30 percent porosity honeycomb is conducted by selecting data run 2 from Figure 5-11 as representative of the 30 percent porosity honeycomb configuration and comparing it to data run 4 from the cylinder no honeycomb configuration. Comparing the cylinder no honeycomb velocity trace in Figure 5-24 and a cylinder no honeycomb velocity variance of 30.65 to the 30 percent porosity honeycomb velocity trace also in Figure 5-24 and a velocity variance of 4.08 from Figure 5-11 continues the trend of porous honeycomb proving its effectiveness at reducing the fluctuating velocity components. Comparing the cylinder no honeycomb mean turbulence intensity of 0.092 from Figure 5-25 to the 30 percent porosity honeycomb mean turbulence intensity of 0.055 also from Figure 5-25 again demonstrates the effectiveness of honeycomb at reducing mean turbulence intensity.

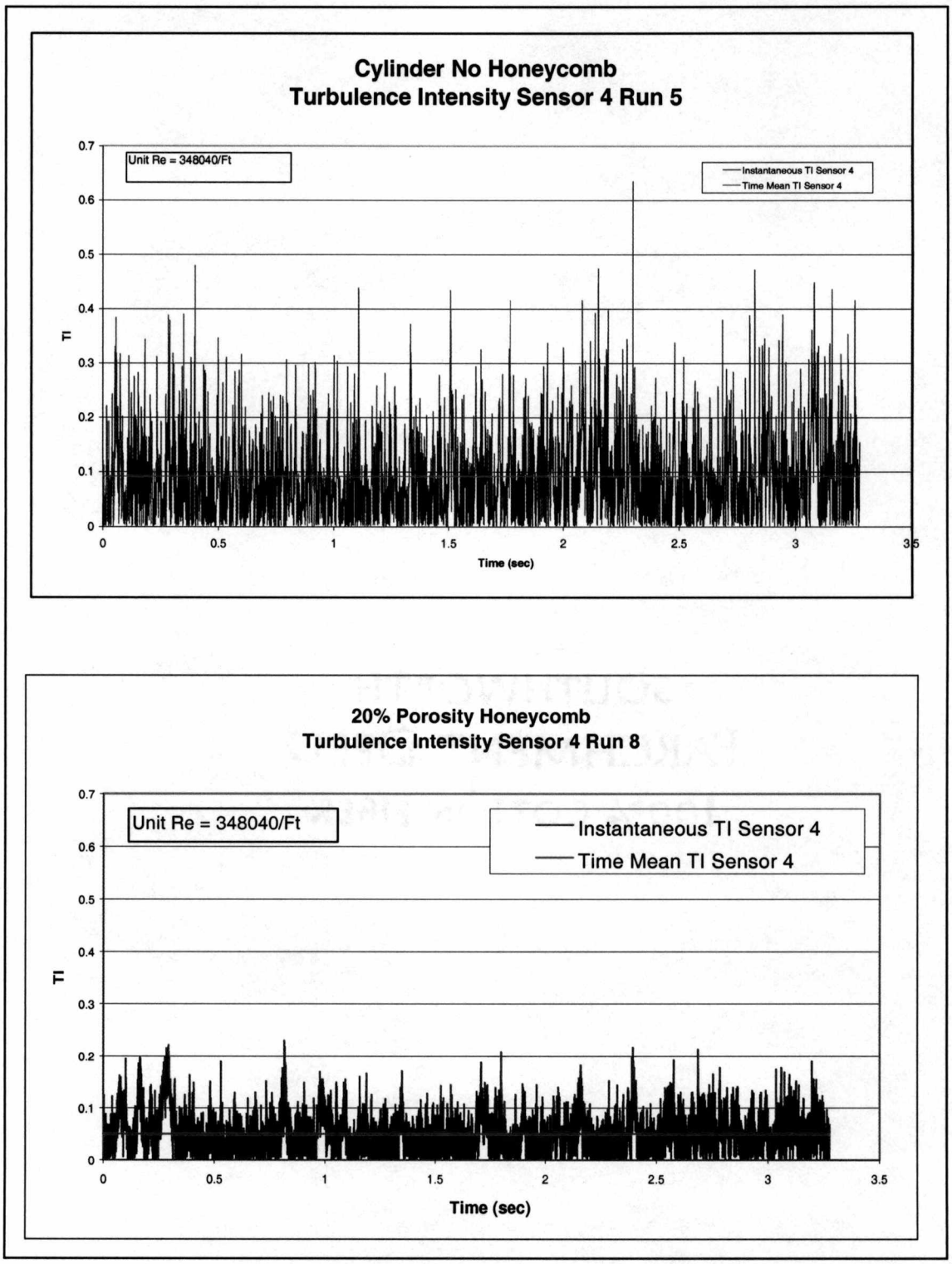


Figure 5-23. Comparison of Cylinder No Honeycomb to 20% Porosity Honeycomb Turbulence Intensity

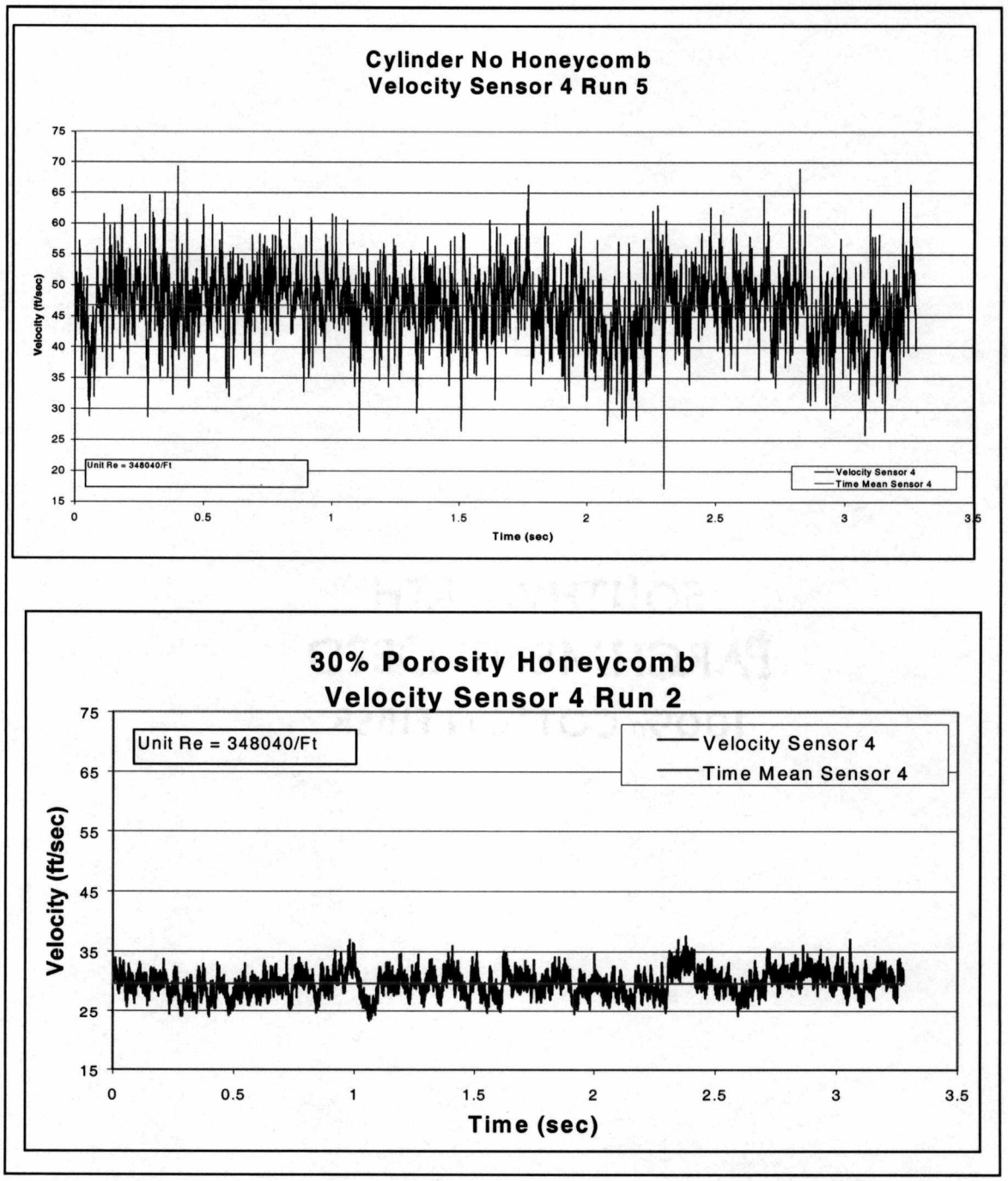


Figure 5-24. Comparison of Cylinder No Honeycomb to 30% Porosity Honeycomb Velocity

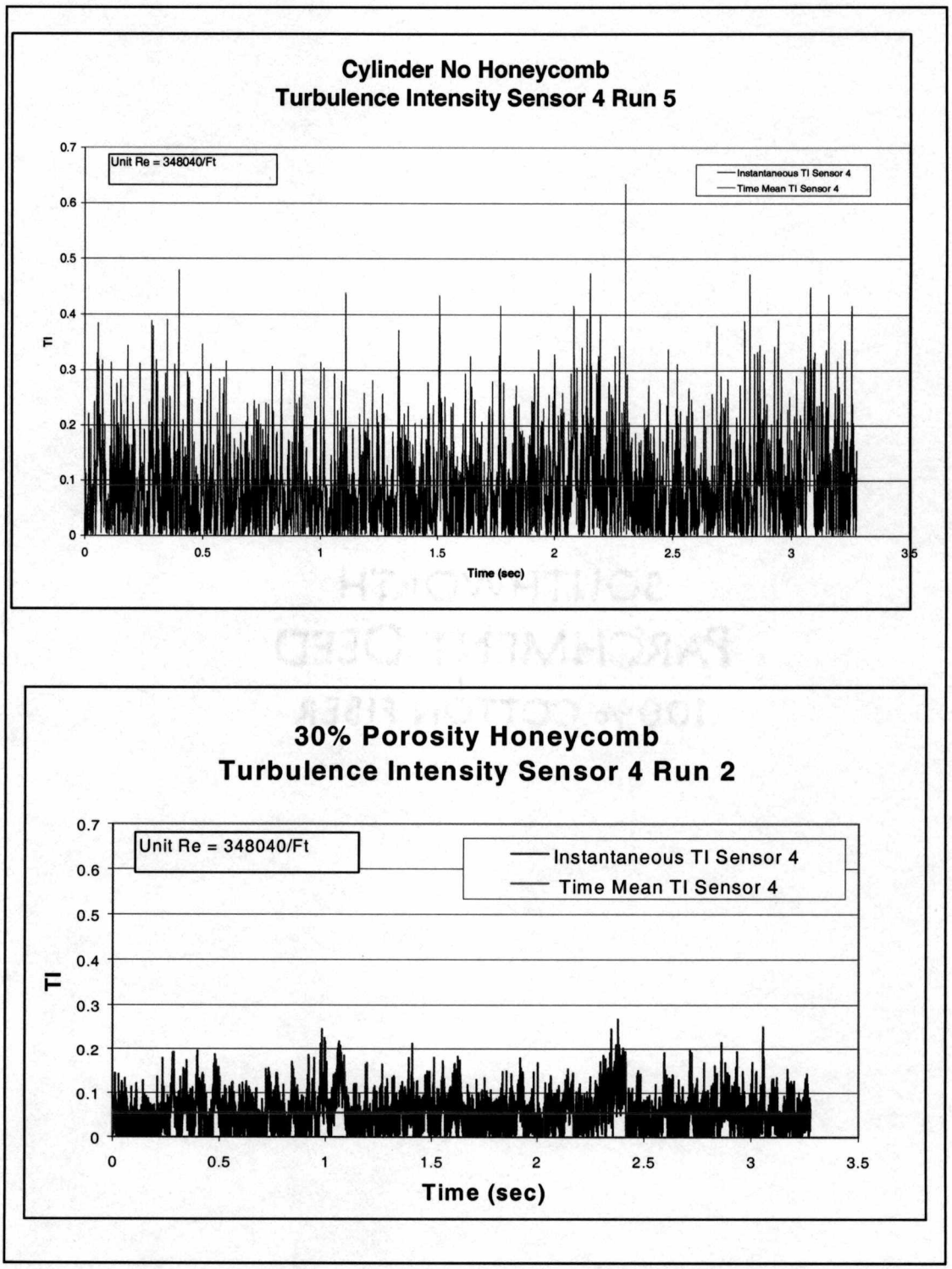


Figure 5-25. Comparison of Cylinder No Honeycomb to 30% Porosity Honeycomb

Turbulence Intensity

Comparison of Cylinder No Honeycomb to 40% Porosity Honeycomb

Finally, the comparison of the cylinder no honeycomb configuration to the 40 percent porosity honeycomb is conducted by selecting data run 7 from Figure 5-13 as representative of the 40 percent porosity honeycomb configuration and comparing it to data run 4 from the cylinder only configuration. Comparing the cylinder no honeycomb velocity trace in Figure 5-26 and a cylinder no honeycomb velocity variance of 30.65 to the 40 percent porosity honeycomb velocity trace also in Figure 5-26 and a velocity variance of 3.76 from Figure 5-13 demonstrates the effectiveness of honeycomb. It also highlights the observation that porous honeycomb has a noticeable improvement over regular honeycomb (6.44 velocity variance) at reducing the fluctuating velocity components. Comparing the cylinder no honeycomb mean turbulence intensity of 0.092 from Figure 5-27 to the 40 percent porosity honeycomb mean turbulence intensity of 0.054 also from Figure 5-27 demonstrates that all four honeycombs successfully reduce mean turbulence intensity.

Comparing the performance of each honeycomb

By averaging the percent turbulence intensity data of each of the eight data runs for each test configuration, a percent turbulence intensity comparison is illustrated in Figure 5-28. Analysis of this data verifies that honeycomb does reduce turbulence and that porous honeycomb is more effective than regular honeycomb at reducing turbulence intensity. The results from Figure 5-28 indicate that the 20 percent porosity honeycomb is most effective. A similar analysis was made for sensor 5 and is summarized in Figure 5-29.

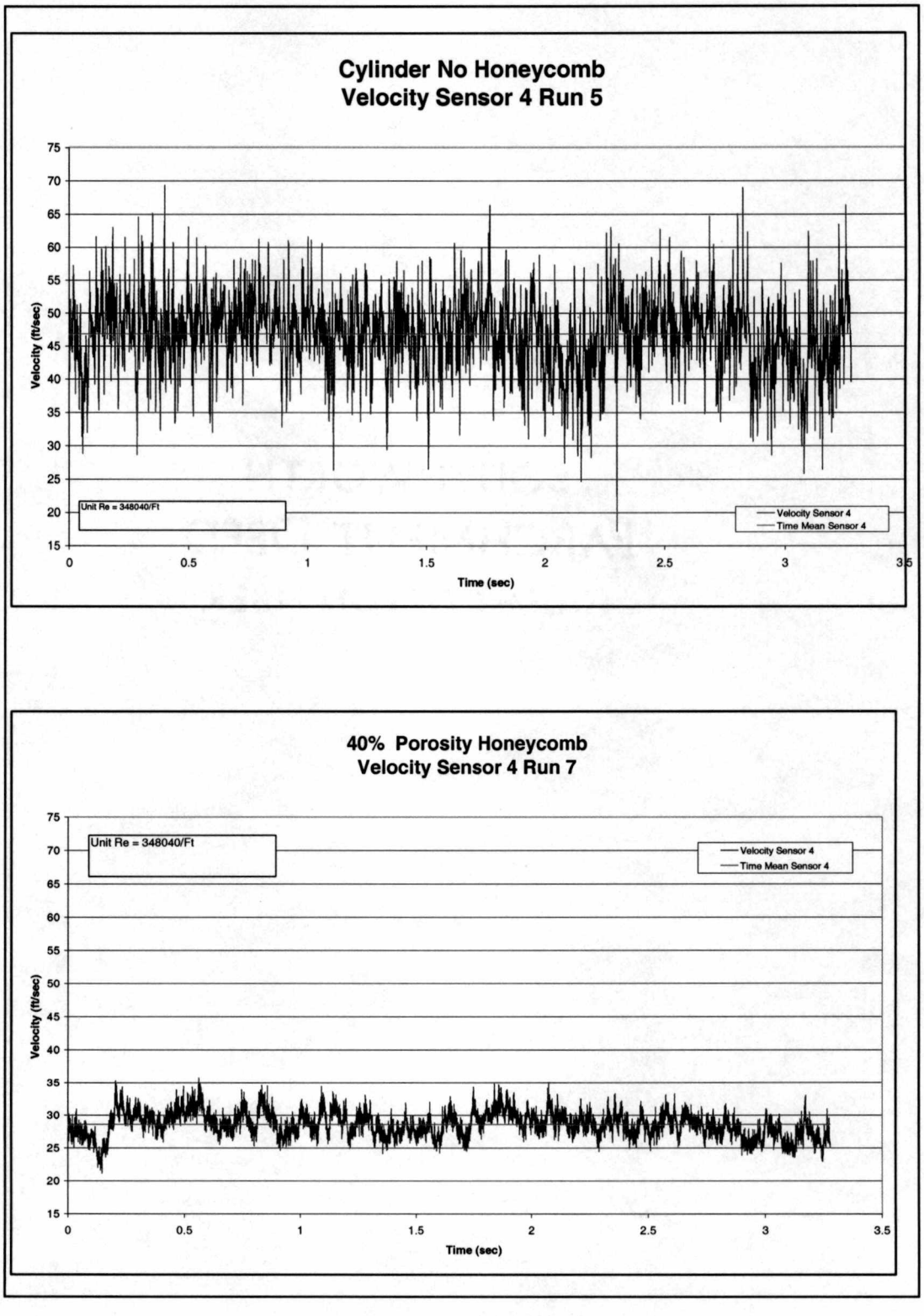


Figure 5-26. Comparison of Cylinder No Honeycomb to 40% Porosity Honeycomb

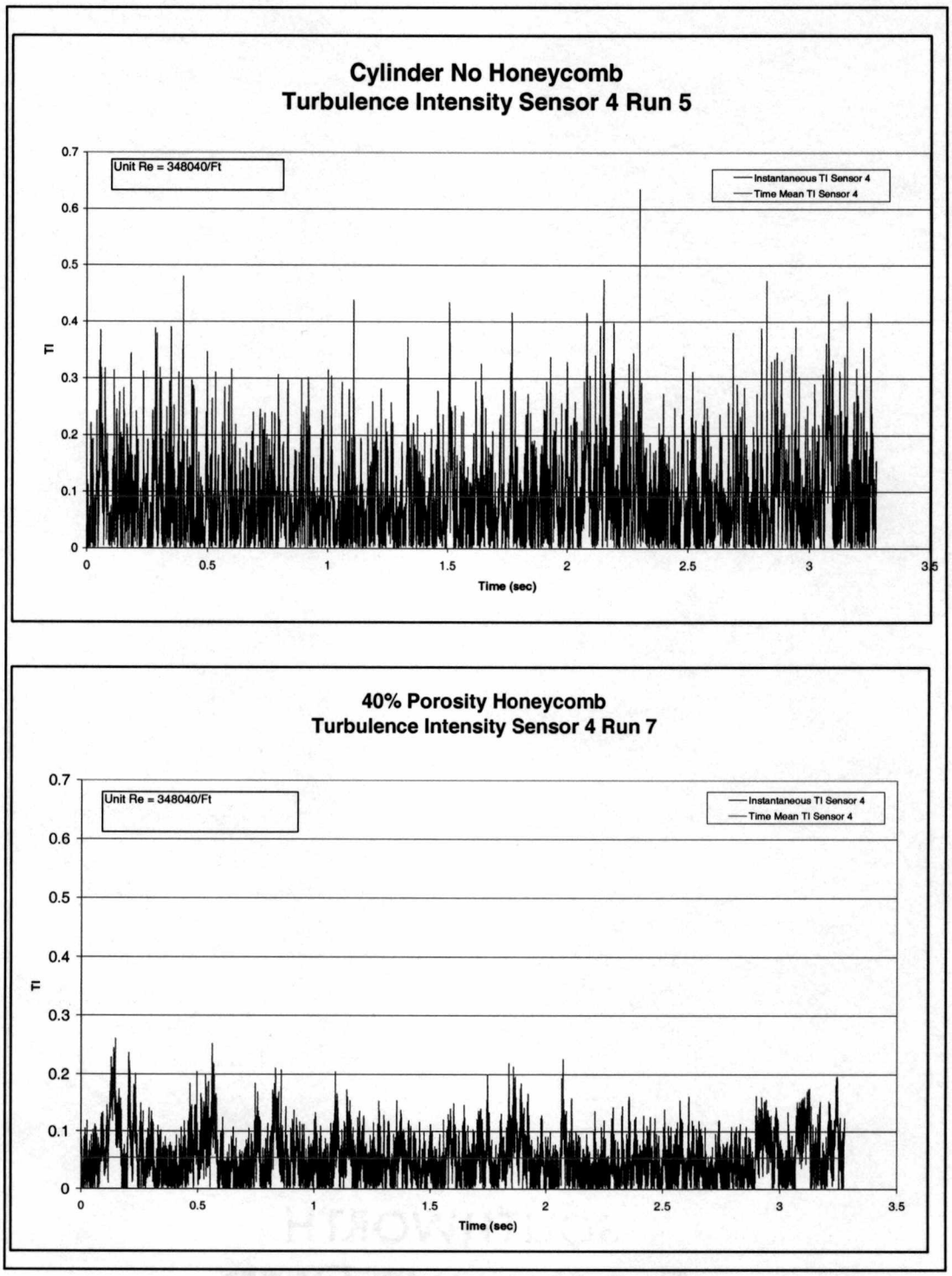


Figure 5-27. Comparison of Cylinder No Honeycomb to 40% Porosity Turbulence Intensity

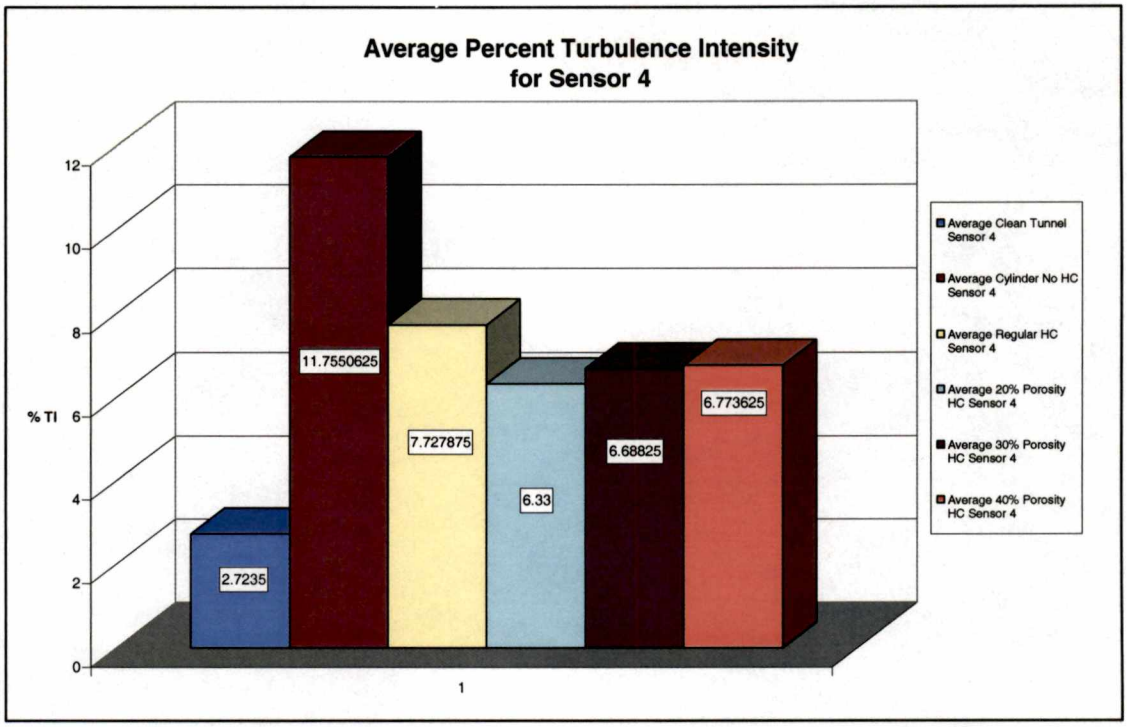


Figure 5-28. Average Percent Turbulence Intensity for Sensor 4

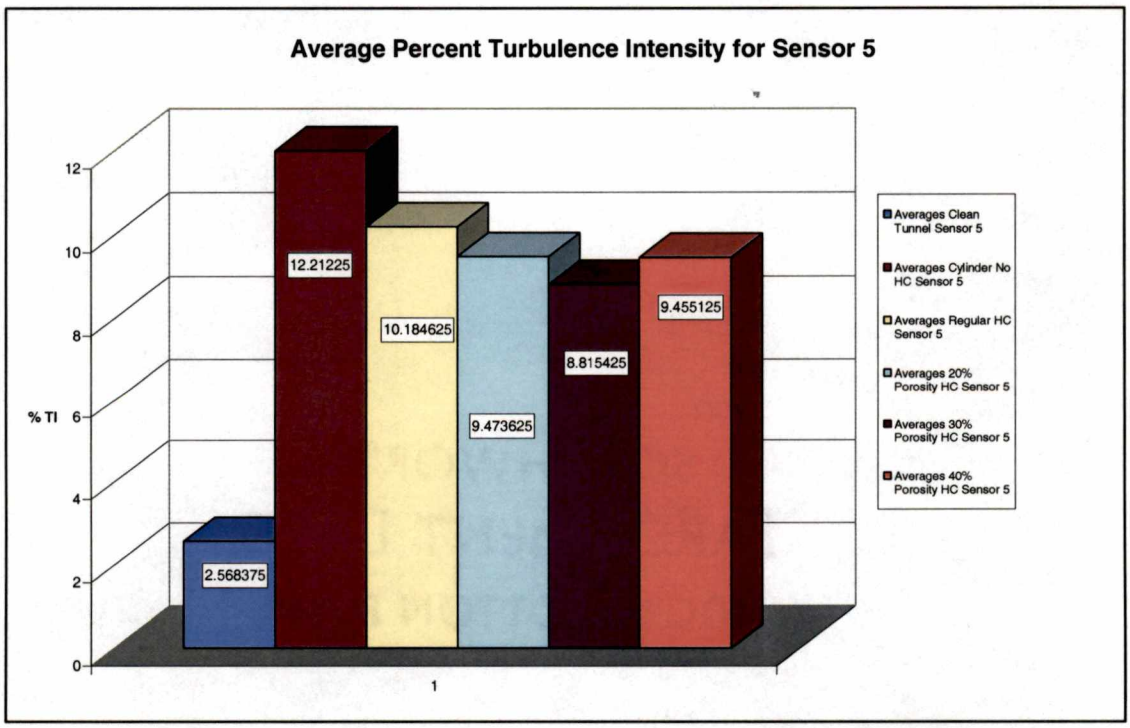


Figure 5-29. Average Percent Turbulence Intensity for Sensor 5

Analysis of this data agrees with sensor 4 data in Figure 5-28 in that porous honeycomb is more effective at reducing turbulence intensity than regular honeycomb. Sensor 5 data indicates that the 30 percent porosity honeycomb is the most effective. As previously mentioned, some caution should be exercised with sensor 5 data due to the suspected wake generated from flow over the top of the honeycomb. Presented in terms of percent improvement of porous honeycomb over regular honeycomb, Table 5-1 highlights the superior performance of porous honeycomb. For sensor 4, the 20 percent honeycomb is an 18 percent improvement in turbulence reduction over regular honeycomb.

Frequency Spectra Results and Analysis

The hot-film sensors collected data up to 2500 Hz. Amplitudes beyond 100 Hz were minuscule. The amplitude data for the clean tunnel is less than 0.02 $(ft/sec)^2/Hz$ across the analyzed spectrum and it is noted that there is not an electrical spike at 60 Hz. The introduction of the cylinder generated large amplitudes relative to the clean tunnel out to about 58 Hz. The large amplitudes are the result of a Karman vortex trail emanating from the cylinder. For the cylinder only, there is a noticeable peak at 50 Hz. The vortex-shedding frequency estimated from the calculated cylinder Strouhal number, in this

Table 5-1. Percent Improvement Over Regular Honeycomb

Honeycomb	Sensor 4	Sensor 5
20% Porosity	18%	7%
30% Porosity	13%	13%
40% Porosity	12%	7%

Reynolds number range, was 69 Hz and does not show up as a significant amplitude at the location of the hot film sensors, which are 26.125 inches down stream of the cylinder.

The analysis of sensor 4 frequency spectrum data in Figure 5-30 and 5-31 indicate that all four honeycombs successfully dampen the Karman vortex trail produced by the cylinder. Focusing on Figure 5-31 in the 0-to-25 Hz range, the performance of all three porous honeycomb varies slightly by frequency with the 20 percent honeycomb having the largest amplitude at 1.2 Hz. The porous honeycomb appears to out perform the regular honeycomb over the 0-to-15 Hz range. Above this range, all four honeycomb approach zero amplitude.

The display of sensor 5 frequency spectrum data in Figure 5-32 and 5-33 shows some larger amplitudes in the 0-to-5 Hz range than sensor 4 detected in the same frequency range. As with the velocity field analysis, this can be attributed to a suspected wake generated from flow over the top of the honeycomb and therefore, sensor 4 data appears to be more reliable.

Analysis of Non-Porous Length to Honeycomb Length

The analysis of the velocity field and frequency spectrum clearly indicates that porous honeycomb is more effective than regular honeycomb at reducing turbulence. However, an analysis of Figure 5-34, which shows percent turbulence intensity against the ratio of non-porous length to total honeycomb length, suggests that there may be an optimum ratio of porous length to total honeycomb length. This ratio, (D_{epa}/D_{LHC}), is a Pi term from the dimensional analysis in Chapter 2. Also, recall in Chapter 2 where the theory of

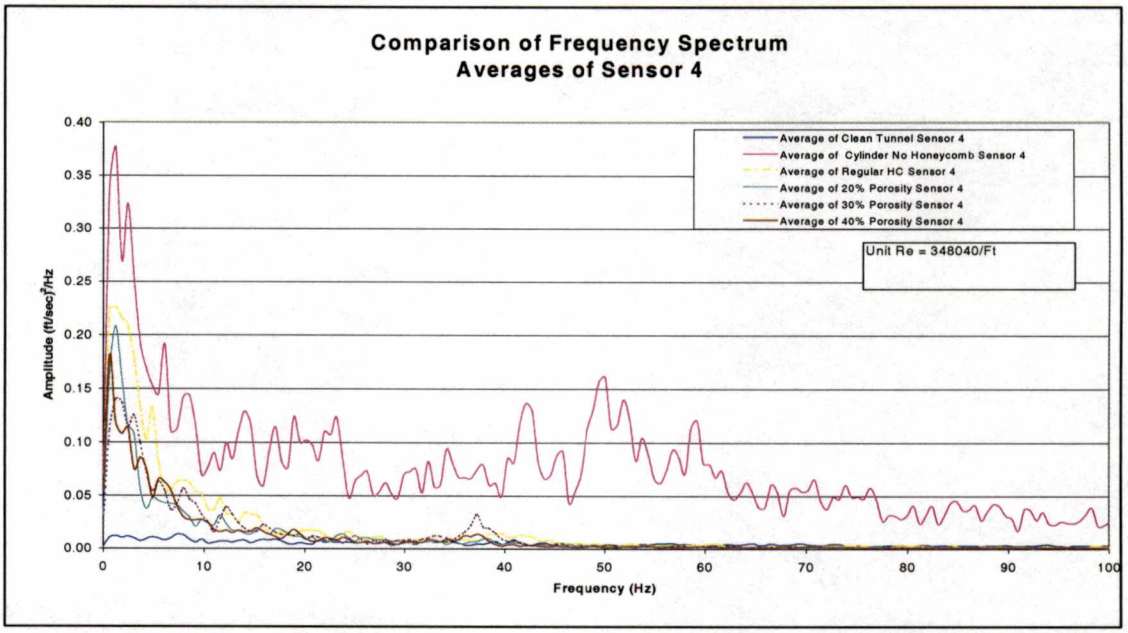


Figure 5-30. Comparison of Frequency Spectrum Averages of Sensor 4, 0 – 100 Hz

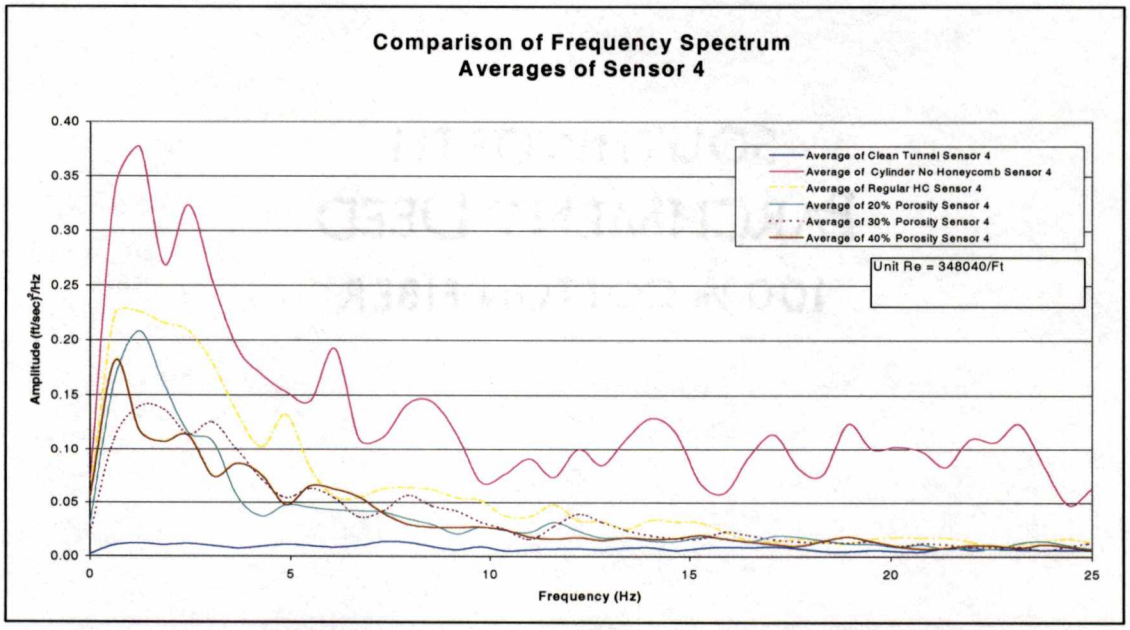


Figure 5-31. Comparison of Frequency Spectrum Averages of Sensor 4, 0 – 25 Hz

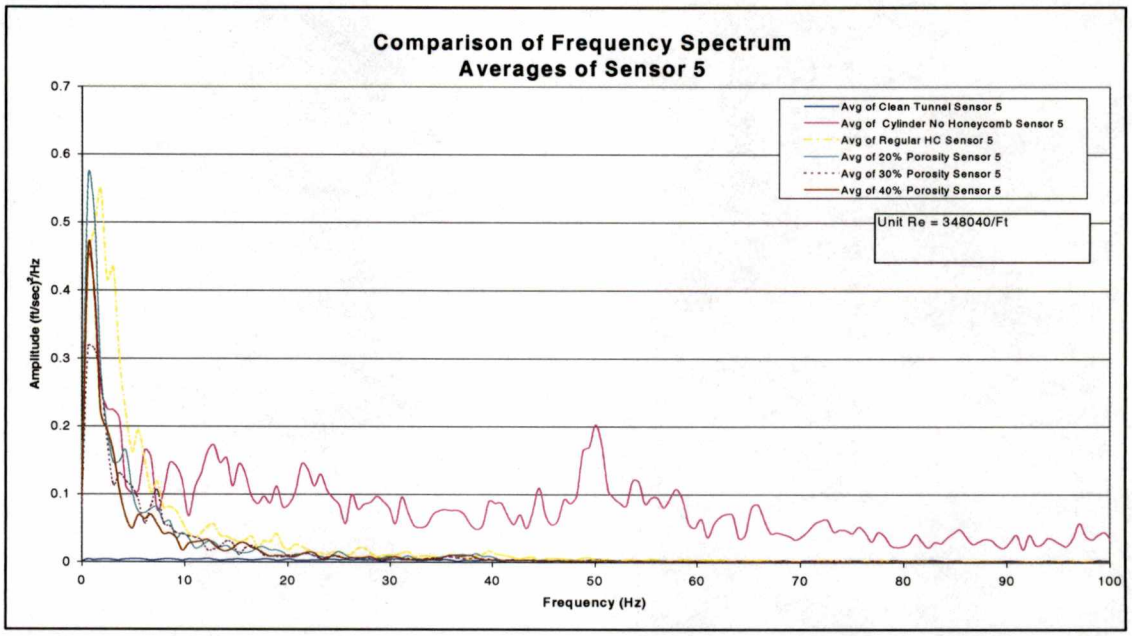


Figure 5-32. Comparison of Frequency Spectrum Averages of Sensor 5, 0 – 100 Hz

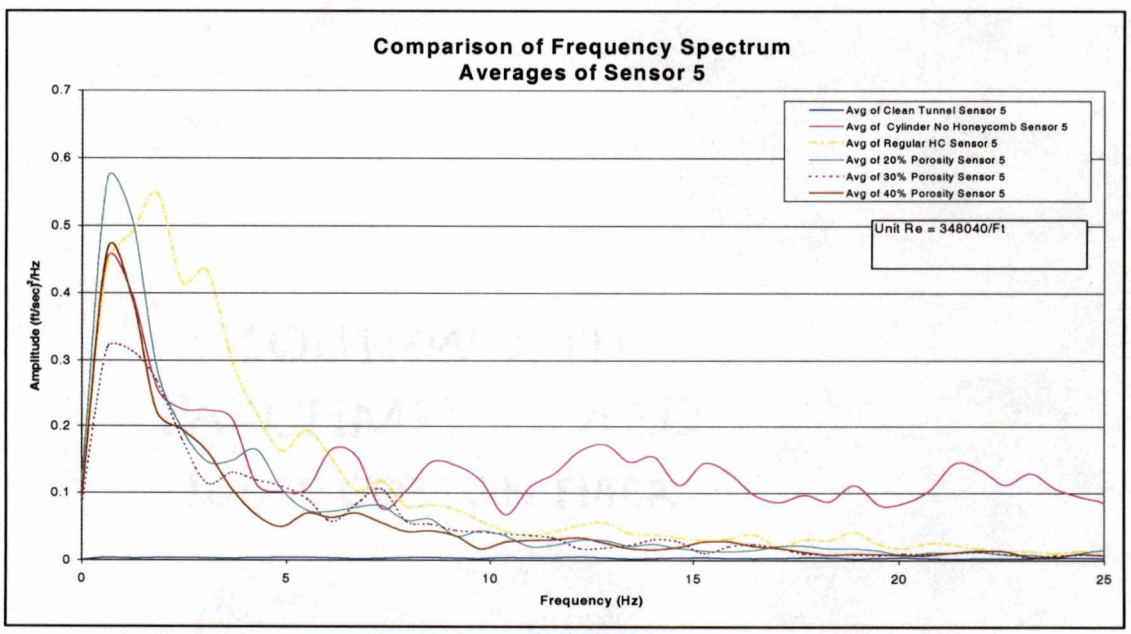


Figure 5-33. Comparison of Frequency Spectrum Averages of Sensor 5, 0 – 25 Hz

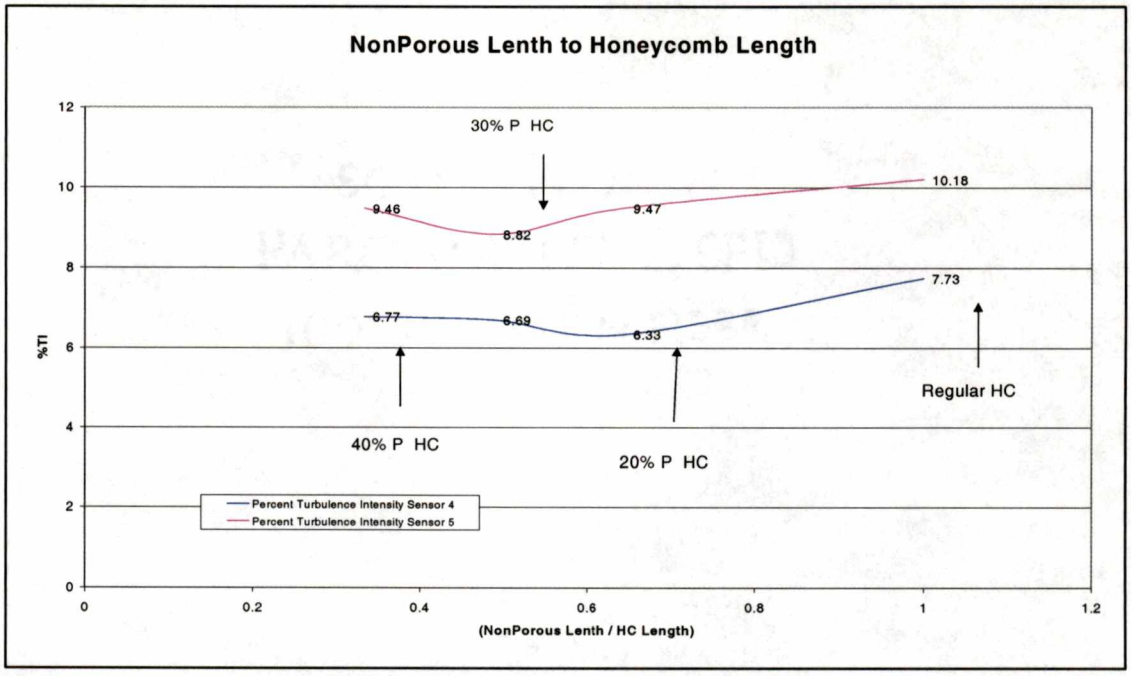


Figure 5-34. NonPorous Length to Honeycomb Length

how honeycomb works mentioned that the walls of each honeycomb cell provide a barrier or mechanism to straighten the flow and therefore reduce lateral velocity components in the flow. Non-porous length to overall honeycomb length ratio data from Figure 5-34 indicates that no more than 50-to-60 percent of the overall length should be porous and that 30-to-40 percent may be optimum. Ergo, as the porous length increases, there is less honeycomb length to perform the traditional flow straightening function of honeycomb.

It is noted that the conclusions from Figure 5-34 are based on a small sample and that one of the many topics of a follow on study and experiment of porous honeycomb could explore the coupling of porous length to non-porous length and its effect on turbulence reduction.

Conclusions for the hot film analysis

The velocity field and frequency spectrum analysis appear to indicate that porous honeycomb is more effective at turbulence reduction than regular honeycomb. Focusing on sensor 4 data, this analysis concludes that porous honeycomb is a 12-to-18 percent improvement over regular honeycomb.

Chapter 6

Conclusions and Recommendations

The purpose of this experiment and study was to perform a comparative study of the effectiveness of porous-cell honeycomb and solid wall honeycomb at reducing large-scale turbulence. Particle image velocimetry and hot film anemometry measurement techniques were employed to perform the experiment and collect data from a regular (solid wall) honeycomb, and from a 20 percent, 30 percent, and 40 percent porous honeycomb. The experiment was conducted at a unit Reynolds number of nearly 350,000 per foot. Both sets of measurements reveal that porous honeycomb may be superior to regular honeycomb at turbulence reduction. The following conclusions are drawn:

- Despite concerns on the difficulty of manufacturing porous cell honeycomb, with craftsmanship and readily available machine shop equipment, the fabrication is not too difficult.
- Comparative measurements and analysis appear to conclude that porous-cell honeycomb is more effective than regular or solid wall honeycomb at reducing upstream turbulence and flow non-uniformity.
- Potential future areas of experiments and study include:

- Solid honeycomb and screen combinations for performance comparison with perforated honeycomb alone.
- Ratio of porous length to total honeycomb length.

List of References

References

1. Dr. Ahmad D. Vakili, Professor University of Tennessee Space Institute
2. Munson, Bruce R., Young, Donald F., and Okishi, Theodore H. Fundamentals of Fluid Mechanics. 2nd Edition. John Wiley & Sons, Inc. 1994.
3. Bouis, X., Prieur, J., Tizard, J. A., and Hefer, G. ETW Aerodynamic Design.
4. Brines, et al – Volume I, NWTC Requirements Specification Release 10.0, CR95-059, 17 Nov 95
5. Rae, William H. and Pope, Alan. Low-Speed Wind Tunnel Testing. John Wiley & Sons, 1984.
6. Lumley, J. L., Passage of a Turbulent Stream Through Honeycomb of Large Length-to-Diameter Ratio's, Journal of Basic Engineering, pages 218-220, June 1964
7. Loehrke, R. I. and Nagib, H. M., Control of Free-Stream Turbulence by Means of Honeycombs: A Balance Between Suppression and Generation, Journal of Fluids Engineering, pages, 342-353, September 1976
8. McKeag, Masters Thesis University of Tennessee, Turbulence Reduction by Wrapped Wire-Mesh Screen, 1996.
9. Goldstein, Richard J. Fluid Mechanics Measurements. Hemisphere Publishing Corporation, 1983.

Appendices

Appendix A

Particle Image Velocimetry Calibration

Particle image velocimetry (PIV) was used to measure the flow field downstream of each honeycomb. The UTSI PIV system consists of two Continuum Nd: YAG lasers, a laser controller for each laser, laser synchronizer, laser telescoping arm, analysis computer, and a PIVCAM 10-30 camera. The PIV technique requires the flow field to be seeded with smoke particles. The technique makes simultaneous measurements of particle velocity vectors using optical imaging techniques. The measurements occur in the plane generated by the laser. This results in two-dimensional vectors. Each time the laser is pulsed, the image of the particles in the laser plane creates an exposure on the camera. Double pulsing the laser gives two images of a particle. By measuring the distance a particle moves and dividing by the time between laser pulses, the velocity a particles in the flow is determined. By measuring the displacements of many particles, the flow field is determined. The PIV is calibrated by setting a measuring scale in the laser plane and focusing the camera on the scale. Next, by selecting a distance on the image of the scale, the PIV software determines the number of pixels in the image and this calibrates future images of seed in the flow.

Appendix B

Hot Film Calibration

Thermal anemometers were used in this experiment to measure velocity. Thermal anemometers operate by sensing heat transfer changes from a thin, electrically heated sensor placed in the flow of study. Their small size and frequency response make them suitable for studying turbulent flow [9. Goldstein, p. 99]. The basic components of a thermal anemometer system are the amplifier, bridge circuit, probe support, sensor and a data acquisitions system. There are two main categories of sensors used with a thermal anemometer system: hot wire and hot film. The hot wire sensor consists of one or more conducting wires with a diameter approximately 4 μm. A hot-film sensor is approximately the same size as a hot-wire sensor, but the hot film has an inner insulating wire for support which is surrounded by a layer of conducting material and a protective film on the outer layer. Since the conducting layer of the hot film is thinner and near the surface, relative to the total cross section of a hot wire, it has a superior frequency [9. Goldstein, p. 133]. A single sensor provides mean velocity and velocity fluctuations. Probes with multiple sensors can provide two and three velocity components. Figure B-1 depicts a single sensor and sensor supports. A turbulent flow field consists of the following orthogonal velocity components with respect to the sensor:

V_N: normal to the sensor and parallel to the supports

V_T: tangent to the sensor

V_{BN}: normal to the sensor and normal to the supports.

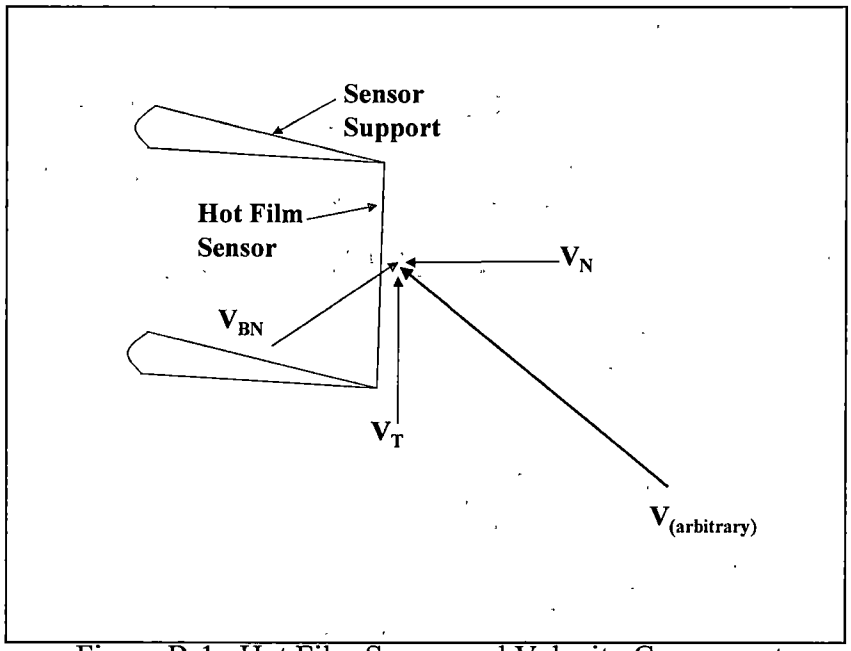


Figure B-1. Hot Film Sensor and Velocity Components

To minimize probe interference, the probe was aligned such that V_{BN} would correspond to the downstream tunnel axis.

The UTSI IFA 300 Thermal Anemometer System was used to calibrate, collect and process the hot film sensor data. Three hot film sensors were calibrated and two were used in the experiment. Sensor data is contained in Table B-1.

Table B-1. Probe Data

Probe Model	Recommended Operating Resistance R_{OP}, Ω	R_{100}-R_0, Ω	R at 0 C, Ω	Internal Resistance R_{int}, Ω
1201-20 #4	8.73	1.23	5.65	0.65
1201-20 #5	8.95	1.29	5.72	0.65
1201-20 #6	8.9	1.27	5.72	0.65

The first step in calibrating the hot-film sensors was to determine the cable resistance. This was measured by shorting the cable and was measured at 0.31 Ω. Next, each sensor was individually calibrated by incrementally increasing the velocity of airflow over the sensor. Figures B-2 and B-3 depict the calibration configuration. During each of the 17 velocity increments, the displacement of a water manometer was also input into the IFA 300 calibration program to provide actual velocities of the flow from an independent measurement. The calibration program calculated the coefficients for a fourth order polynomial curve for each sensor. The IFA 300 used the calibration curves during the experiment to determine velocity from measured voltage. The fourth order polynomial has the following form:

Velocity(Probe) = G + HE + IE^2 + JE^3 + PE^4

where E is the measured voltage and G, H, I, J, and D are the coefficients. The calibrated polynomial for each sensor is as follows:

V4= -123.93 + 301.06 * E –265.41 * E^2 + 98.83 * E^3 –12.29 * E^4

V5= 6.72.- 3.42 * E –6.46 * E^2 + 3.03 * E^3 + 0.72 * E^4

V6= 5.94 – 3.12 * E –5.79 * E^2 + 2.54 * E^3 + 0.85 * E^4

Figures B-2, B-3 and B-4 depict the calibration curves for each sensor.

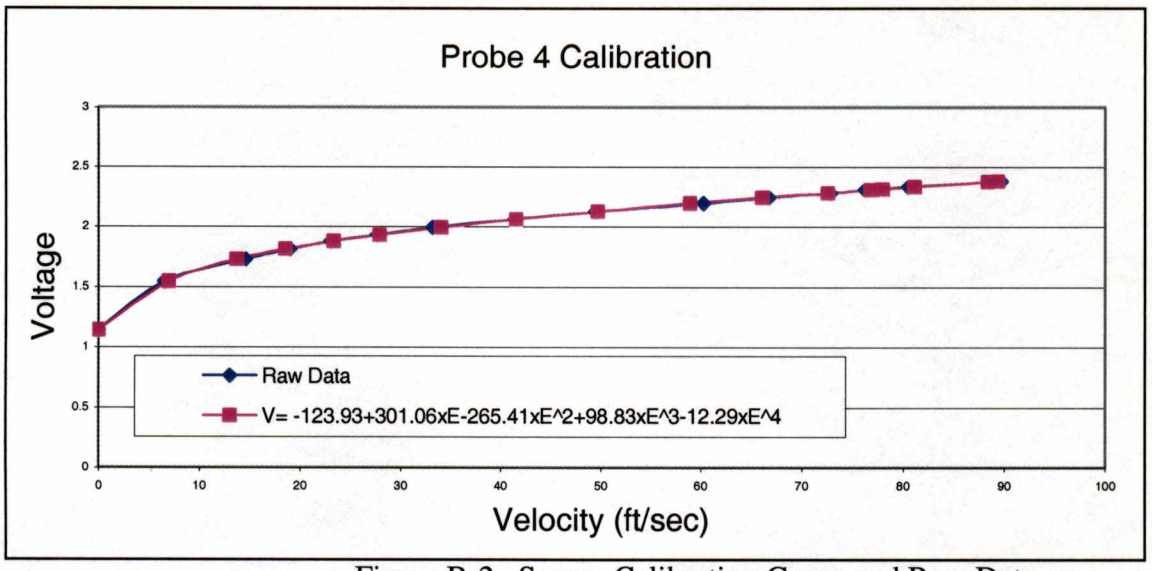


Figure B-2. Sensor Calibration Curve and Raw Data

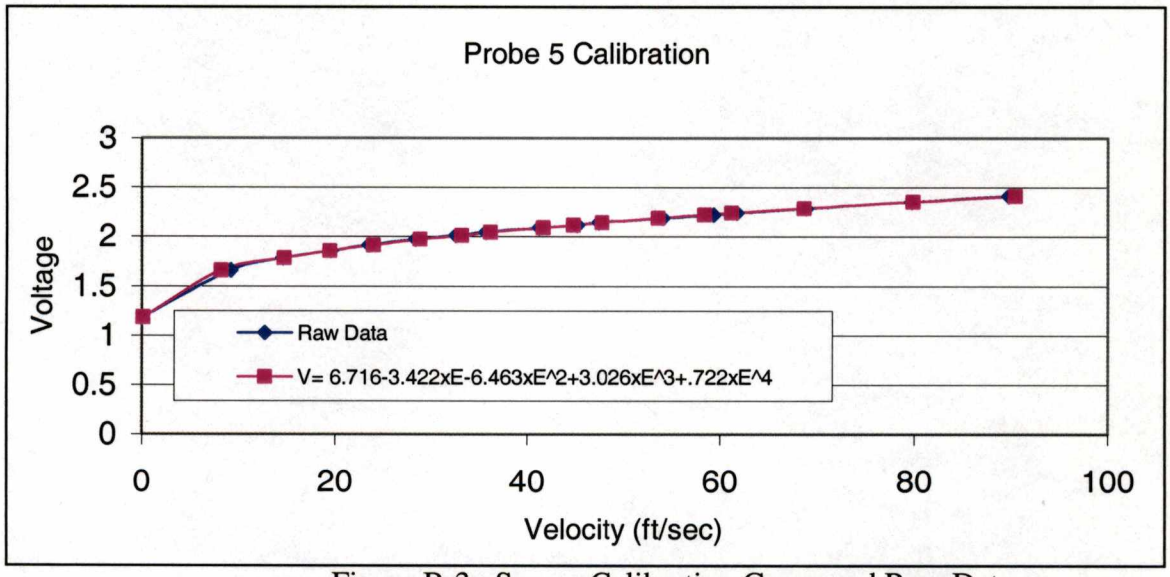


Figure B-3. Sensor Calibration Curve and Raw Data

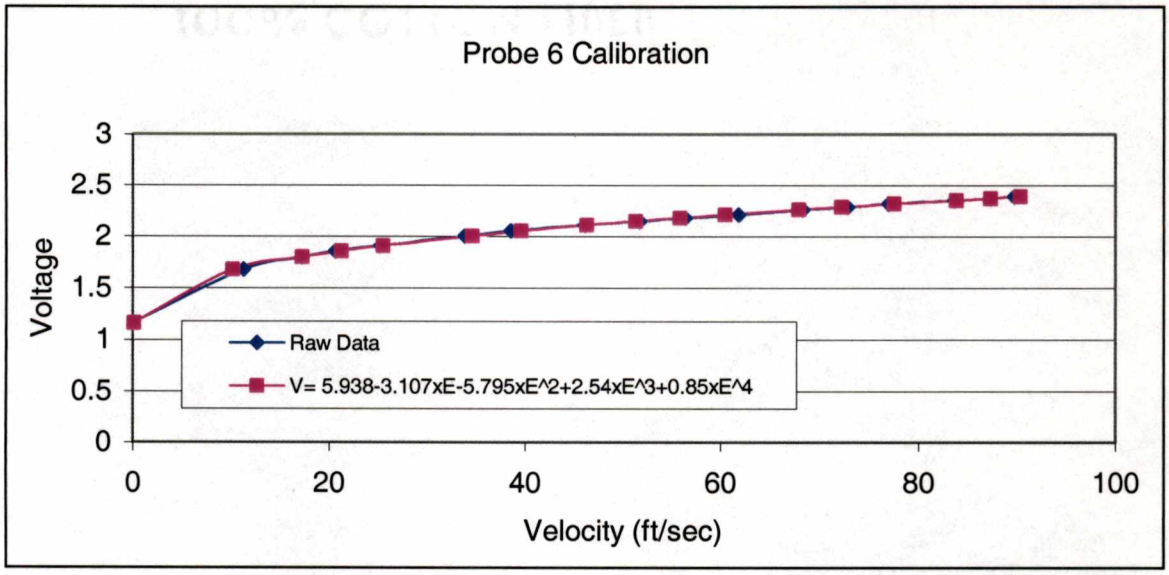


Figure B-3. Sensor Calibration Curve and Raw Data

Vita

Trey Elder was born in Winchester Tennessee and graduated from Tullahoma High School in 1984. He then attended the University of Tennessee where he received a Bachelor of Science in Engineering Science and was commissioned a 2nd Lieutenant in the United States Air Force in 1989. He also earned a Master of Science in International Relations from Troy State University in 1994. After his commission, Lt Elder was assigned to Eglin Air Force Base where he served as a program manager in combat training systems and as a program manager for aircraft weapon and stores testing. Captain Elder's next assignment was to Arnold Air Force Base where served a variety of positions to include cost analyst, chief commander's action group and as an aerospace engineer in Arnold's Technology Division. Captain Elder was then selected to be an instructor at Squadron Officer School and at the Aerospace Basic Course at Air University, Maxwell Air Force Base. Major Elder is currently assigned to Hanscom Air Force Base as a program manager for joint force experimentation.